

## Metamorphic reactions related to decompression and synkinematic intrusion of leucogranite, High Himalayan Crystallines, Bhutan

C. DAVIDSON,<sup>1\*</sup> D.E. GRUJIC,<sup>2†</sup> L. S. HOLLISTER<sup>3</sup> AND S. M. SCHMID<sup>4</sup>

<sup>1</sup>Department of Geological and Geophysical Sciences, Princeton University, Princeton, NJ 08544, USA

<sup>2</sup>ETH Zentrum, Geologisches Institut, CH-8092 Zürich, Switzerland

<sup>3</sup>Department of Geosciences, Princeton University, Princeton, NJ 08544, USA

<sup>4</sup>Geologisches Institut der Universität, Bernoullistrasse 32, CH-4056 Basel, Switzerland

**ABSTRACT** The High Himalayan Crystallines (HHC) of Bhutan were penetratively deformed, intruded by leucogranite and metamorphosed during the collision of the Indian and Asian plates. Metamorphic reaction textures in the HHC show that it experienced decompression while maintaining a laterally heterogeneous, and locally inverted, internal temperature range of c.600–750 °C. This thermal structure was produced by thrusting hot, migmatitic rocks over lower-grade rocks within the HHC and by the advection of heat from the intrusion of leucogranite dykes and sills during decompression. A variable velocity field within the HHC during exhumation and extrusion between India and Tibet caused the inversion of top to the south sense of shear present throughout most of the HHC to top down to the north shear near its top.

**Key words:** Bhutan Himalaya; decompression reactions; Himalayan metamorphism; petrogenetic grid; synkinematic leucogranite.

### INTRODUCTION

The High Himalayan Crystallines (HHC) are a penetratively deformed and metamorphosed portion of the Indian Shield and its Precambrian and Palaeozoic cover rocks, which form a nearly continuous belt along the Himalayan chain (Heim & Gansser, 1939; Gansser, 1964; LeFort, 1975; Windley, 1983). Most workers agree that the HHC were deformed, metamorphosed, intruded by leucogranite and exhumed during the ongoing collision of India and Asia. However, the relationship between (and relative importance of) these different processes is an outstanding problem in Himalayan tectonics (see articles in Treloar & Searle, 1993).

Most of the regional-scale tectonic subdivisions of the Himalaya (including the HHC) were first described by Heim & Gansser (1939) and Gansser (1964). They showed that the HHC were thrust over the sedimentary rocks of the Lesser Himalaya across the Main Central Thrust (MCT) (Fig. 1). Heim & Gansser (1939) stressed that in most places the MCT is not well defined, but rather is a diffuse zone where metamorphism in the sedimentary rocks of the Lesser Himalaya increases upwards towards the overlying biotite gneisses of the HHC. Nevertheless, the MCT, as mapped by them, represents a protolith boundary

separating the gneissic basement of the HHC from the sediments of the Lesser Himalayas.

The contact of the HHC with the overlying Tethyan sedimentary rocks was originally described as a 'normal' sequence with a rapid decrease in metamorphic grade from the HHC into the overlying sedimentary rocks (Heim & Gansser, 1939; Gansser, 1964). However, in southern Tibet, Burg *et al.* (1984) showed that the Tethyan rocks are tectonically juxtaposed against the underlying HHC along a N-dipping fault zone with normal displacement. Burchfiel *et al.* (1992) called this fault zone the South Tibetan Detachment System (STDS) and described it in many areas along the Himalayan chain including southern Tibet and Bhutan.

Since the work of Heim & Gansser (1939), the metamorphic history of the HHC has received much attention (e.g. see special issue of the *Journal of Metamorphic Geology* edited by Barnicoat & Treloar, 1989). Of particular interest is the presence of an inverted metamorphic field gradient within the HHC, where high-grade metamorphic rocks and migmatite (containing sillimanite, K-feldspar, and cordierite) occur structurally above lower-grade rocks (containing staurolite and kyanite). The inverted nature of the metamorphic gradient is confirmed in areas with sufficient 3-D control, such as the half-window of the Kuru Chu-Shumar spur near Mongar, Bhutan (Fig. 1), the Kistwar window, Nepal (Jain & Manickavasagam, 1993), and the Ranjit window of the Darjeeling–Sikkim Himalaya (Mohan *et al.*, 1989; Fig. 1). In addition, leucogranite dykes and sills occur throughout the HHC, but the large Tertiary-age leucogranite

\*Present address: Department of Geology, Beloit College, Beloit, Wisconsin 53511 (email: davidson@beloit.edu).

†Present address: Albert-Ludwigs Universität, Geologisches Institut, Albertsstrasse 23-B, D-79104 Freiburg i.Br., Germany.

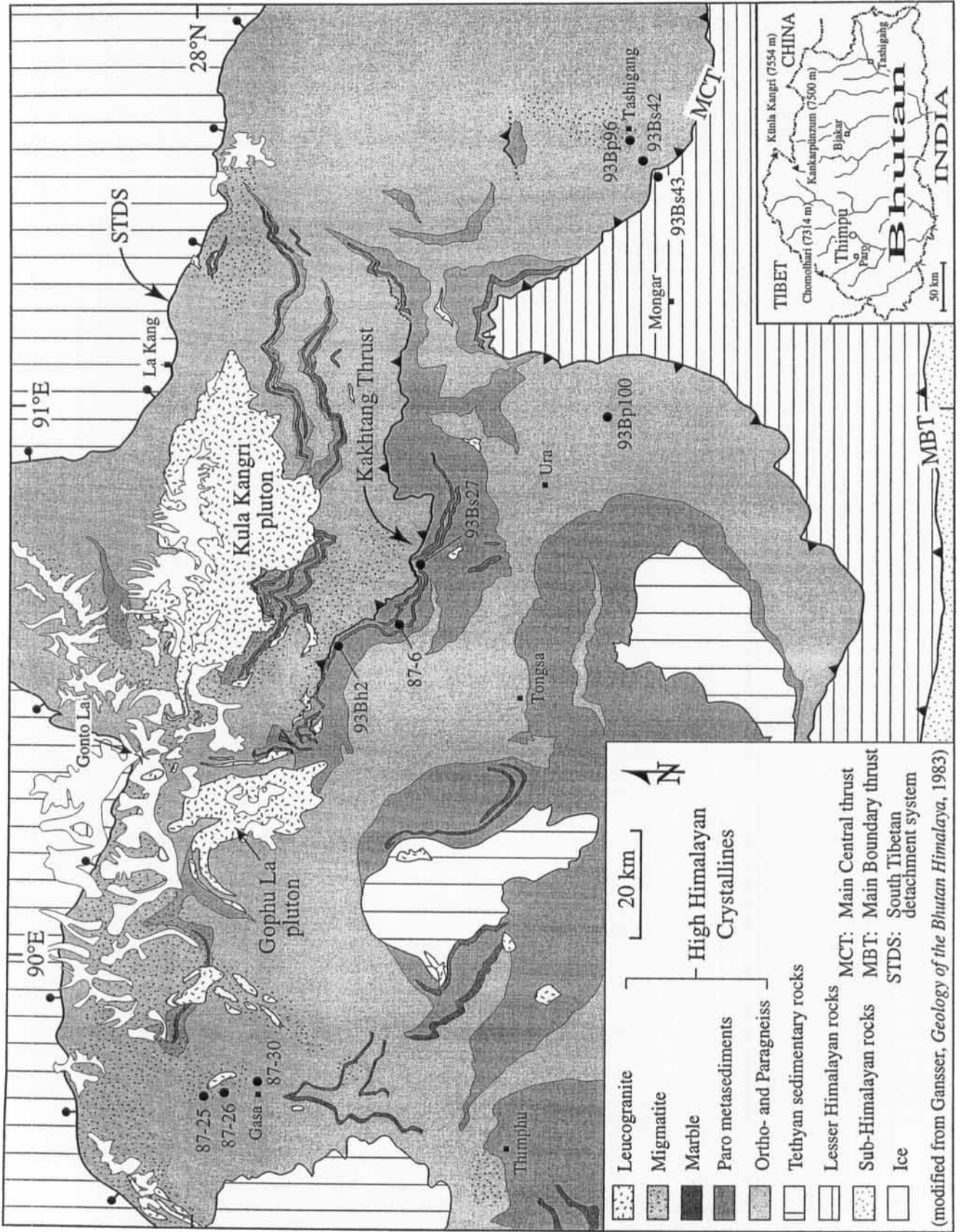


Fig. 1. Simplified geological map of Bhutan (modified from Gansser, 1983). Sample locations referred to in text are indicated by filled circles and labelled.

plutons (Fig. 1) are restricted to the highest structural levels. The unique geochemistry of these plutons shows that they were derived entirely from partially melted crustal material (LeFort *et al.*, 1987).

A number of tectonic models (discussed later) have been proposed for the generation of the leucogranites and to explain the inverted metamorphic field gradient in the HHC (for reviews see Windley, 1983; Searle & Rex, 1989; Jain & Manickavasagam, 1993; Jaupart & Provost, 1985). Many of these models rely on geothermobarometric results obtained from different structural levels within the HHC (e.g. Hodges *et al.*, 1988a,b; Hubbard, 1989; Pêcher, 1989; Swapp & Hollister, 1991; Searle *et al.*, 1992; Jain & Manickavasagam, 1993). However, based on our work in the HHC of Bhutan, we question if geothermobarometry can be used reliably to test tectonic models for the formation and preservation of the inverted metamorphic field gradient because equilibrium assemblages are rarely preserved. Furthermore, it is emphasized that a structurally upward-increasing grade of metamorphism does not necessarily imply inverted isotherms at a given instant of time during the orogenic evolution (e.g. LeFort, 1975; Jamieson *et al.*, 1996).

In this paper we describe metamorphic reactions preserved in the HHC of Bhutan that demonstrate that the region underwent decompression at high temperature, associated with the partial consumption of garnet. Garnet in these rocks typically has irregular and/or truncated zoning patterns, indicating that equilibrium with the matrix was not maintained during decompression. We show that leucogranite was intruded into the HHC during penetrative top to the south shearing and that some increase of temperature during decompression was due to these intrusions.

## GEOLOGICAL SETTING

Bhutan is approximately the size of Switzerland, with elevations ranging from less than 300 m in the south to over 7500 m in the north. Most of the rocks in Bhutan are part of the High Himalayan Crystallines (HHC), consisting of orthogneiss and subordinate paragneiss (undifferentiated), the Paro metasedimentary rocks, migmatite and leucogranite (Fig. 1). Gansser (1983; p. 119) described the leucogranite as being 'generally medium to fine grained, very homogeneous and mostly massive.' He showed that the leucogranite and probably most of the migmatite are Tertiary in age (Gansser, 1983), and argued for Palaeozoic and/or Pre-Palaeozoic protolith ages for the gneisses and Paro metasedimentary rocks. Besides the large leucogranite plutons in the northern part of the HHC (Fig. 1), leucogranite dykes and sills occur throughout the HHC. The Paro metasedimentary rocks contain metapelite, marble, calcsilicate, and quartzite (Gansser, 1983). In Fig. 1, some of the large marble horizons, as mapped by Gansser (1983), are shown in dark grey.

In 1993 a Swiss-American expedition to Bhutan evaluated the role of leucogranite in the deformation and metamorphism of the Bhutan Himalayas, and searched for a major thrust fault (the Kakhtang thrust) predicted by Swapp & Hollister (1991). The samples described in the present study were collected by the expedition team. We found that many of the marble layers mapped by Gansser contain a large percentage of leucogranite, and in a few places the mapped marbles are actually leucogranite sills. Gansser (1983) pointed out the close association of the marble horizons and leucogranite sills, but apparently mapped most of these rocks as marble.

Gansser (1983) reported Rb–Sr and K–Ar biotite and muscovite dates from a variety of rock types. With the exception of a 26 Ma Rb–Sr muscovite date from Tashigang (Fig. 1), the ages are between 13 and 9 Ma. Maluski *et al.* (1988) reported concordant 11 Ma biotite and muscovite  $^{39}\text{Ar}$ – $^{40}\text{Ar}$  dates from two samples from the Kula Kangri pluton (Fig. 1). They described these samples as having a mylonitic fabric with recrystallized biotite and muscovite. Ferrara *et al.* (1991) dated muscovite and biotite (Rb–Sr) from two samples from the Gophu La pluton (Fig. 1). These samples yielded slightly discordant dates ranging from 15.1 to 14.0 Ma. To our knowledge, no U–Pb dates have been published for any of the rocks from Bhutan. However, Deniel *et al.* (1987) reported two U–Pb monazite dates of 25 Ma for the Manaslu pluton in Nepal. Taken together, these data show that the HHC of Bhutan cooled from high temperature by the end of Mid-Miocene times. However, the scarcity of geochronological data, especially from the lower structural levels of the HHC, precludes a detailed analysis of the cooling history at this time. To address this problem, a 1996 expedition to Bhutan, led by Hollister, collected geochronology samples from the lower structural levels.

Most of the rocks in the HHC have a well-developed foliation defined by the shape preferred orientation of micas. The foliation generally dips gently to the north, but is warped on a regional scale about both N–S- and E–W-trending axes (see structural map of Gansser, 1983). Stretching lineations typically plunge to the north and kinematic indicators show that the direction of transport throughout most of the HHC was to the south (Swapp & Hollister, 1991; Grujic *et al.*, 1996), which is common along the entire Himalaya (e.g. Bouchez & Pêcher, 1981; Brunel, 1986; Gansser, 1983; Jain & Manickavasagam, 1993; Reddy *et al.*, 1993). We refer to this wide zone of distributed top to the south shearing within large portions of the HHC, including shearing at the MCT, as the Main Central Thrust Zone (MCTZ). The MCTZ is distinct from the MCT which is a protolith boundary between units of the HHC and the sediments of the Lesser Himalaya (Fig. 1).

Burchfiel *et al.* (1992) described a complex stratigraphy and structural history at the top of the HHC and overlying Tethyan sedimentary rocks at La Kang, near the northern border of Bhutan (Fig. 1). They showed

evidence for an early phase of top to the south thrusting overprinted by a top down to the north shear fabric. They also showed that the Khula Kangri pluton intruded during this later deformation event, in places being caught up in the deformation, while in other places cutting all fabrics and obscuring the contact between the HHC and overlying Tethyan rocks. Edwards *et al.* (1996), working west of La Kang at Gonto La (Fig. 1), described a less complicated contact between the HHC, leucogranite and Tethyan rocks. At Gonto La, a large leucogranite body, assumed to be part of the Khula Kangri pluton, intruded mylonitic rocks of the HHC containing deformed leucogranite dykes and sills. The mylonitic foliation in these rocks is parallel to the pluton contact, with top down to the north sense of shear indicators. The pluton and mylonitic complex are truncated by a younger brittle normal fault which places Tethyan rocks on top of these rocks with top down to the north displacement.

To summarize, the HHC of Bhutan is a penetratively deformed group of rocks with top to the south shear fabrics overprinted by top down to the north shear fabrics in the highest structural levels. It is bounded by the north-dipping MCT in the south, and the north-dipping South Tibetan detachment system in the north (Fig. 1).

#### Overview of the metamorphism

Swapp & Hollister (1991) gave an overview of the metamorphic rocks found in Bhutan based on the previous work by Gansser (1983) and their own observations. Based on differences in metamorphic history and structural position within the HHC, the studied rocks were assigned to either the high structural levels or the low structural levels. Rather than repeating the Swapp & Hollister (1991) discussion here, their observations are briefly summarized, with some modification based on observations resulting from the Swiss–American expedition to Bhutan in 1993. We focus on the metapelitic rocks that occur in the Paro metasedimentary rocks and in the undifferentiated gneisses (Fig. 1). These metapelites contain quartz, plagioclase and biotite; muscovite, garnet, sillimanite and/or kyanite are common. Migmatitic texture is

present in all structural levels but is more common in the higher structural levels. Massive sillimanite, K-feldspar and cordierite occur in the higher structural levels. In the lower structural levels staurolite, kyanite and fibrolitic sillimanite are found. These differences in mineralogy and texture between the higher and lower structural levels define an apparent inverted metamorphic field gradient (Swapp & Hollister, 1991).

Metamorphic reaction textures are common in these rocks (discussed below), and the timing of deformation relative to the growth of the metamorphic minerals is complex (Gansser, 1983; Swapp & Hollister, 1991). In the lower structural levels, staurolite and garnet locally are poikilitic and have spiral inclusion trails showing they grew during deformation (93Bs27, Fig. 2a). In some locations (e.g. near 93Bp100, Fig. 1), kyanite is aligned with the foliation, is bent and clearly pre-dates or is synchronous with the main foliation (see fig. 3b in Swapp & Hollister, 1991). In other locations, fibrolitic sillimanite forms mats around garnet and is apparently post-kinematic (87–6, see fig. 3c in Swapp & Hollister, 1991), and in yet other locations, fibrolitic sillimanite is aligned with the foliation, grows in the pressure shadows of garnet and is probably synkinematic (93Bp45, Fig. 2b). In most of these rocks, garnet has irregular or rounded margins suggesting dissolution, and, locally, the crystals appear to have been truncated (93Bp96, Fig. 2c). In the high structural levels, biotite and sillimanite (when present) define the foliation. Spiral inclusion trails in garnet are rare or absent, and cordierite (when present) appears to be undeformed. Kyanite is found in the high structural levels only as inclusions in garnet (Fig. 2f).

Overall, these relationships show that metamorphism and deformation in the HHC of Bhutan were synchronous. However, in detail, the growth of metamorphic minerals in some areas pre-dates and in other areas post-dates the main foliation-forming event.

#### METAMORPHIC REACTION TEXTURES

The metapelitic rocks of Bhutan contain a wealth of spectacular metamorphic reaction textures (Swapp & Hollister, 1991; this study). Mineral assemblages are given in Table 1 with sample locations shown in Fig. 1.

**Fig. 2.** Photomicrographs from the HHC of Bhutan. (a) Sample 93Bs27: spiral inclusion trails in garnet and staurolite. (b) Sample 93Bp45: sillimanite and biotite in pressure shadows of garnet. Note how garnet margins appear to have been partially consumed. This texture suggests that reaction (5) (Table 2) took place in this rock. (c) Sample 93Bp96: truncated garnet. Note how quartz inclusions define a semi-circular trace inside the garnet, which appears to have been truncated along its lower margin. This suggests that this rock was deformed after garnet growth. (d) Sample 93Bp100: biotite growing in pressure shadows between garnet and muscovite, and subhedral staurolite growing at garnet rim. See Fig. 3(c) for a close-up view of the garnet. This texture suggests that reaction (1) (Table 2) took place in this rock. (e) Sample 93Bh2: staurolite and sillimanite inclusion in garnet. Staurolite inclusions in garnet are not uncommon in the HHC. In this rock, sillimanite and minor amounts of corroded staurolite fragments occur in the matrix suggesting that reaction (2) (Table 2) took place. (f) Sample 87–25: kyanite inclusion in garnet. (g) Sample 87–25: coarse-grained sillimanite. The matrix of this rock is mostly sillimanite, biotite, K-feldspar and quartz (no muscovite); kyanite is found only as inclusions in garnet. These textures suggest that reactions (4) and (6) (Table 2) took place in this rock. (h) Sample 93Bp96: biotite in pressure shadows between garnet and muscovite. Sillimanite occurs in the matrix and is parallel to the foliation. Note how the garnet margin in contact with biotite has apparently been consumed, probably due to reaction (5) (Table 2). (i) Sample 87–30: cordierite and K-feldspar partially replacing biotite and sillimanite. This texture suggests that reaction (7) (Table 2) took place in this rock.

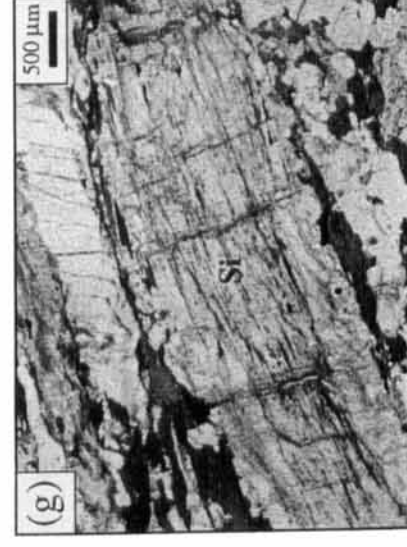
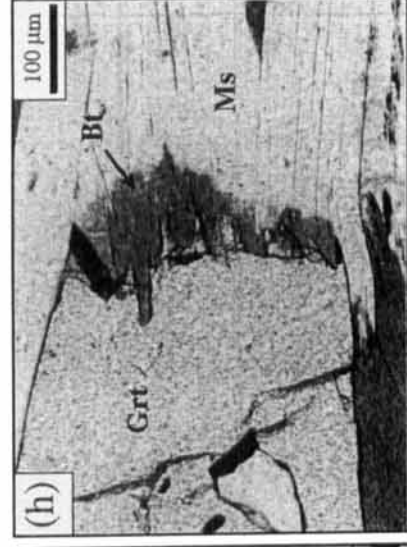
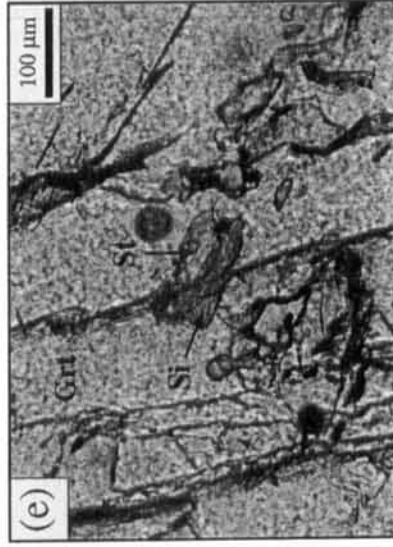
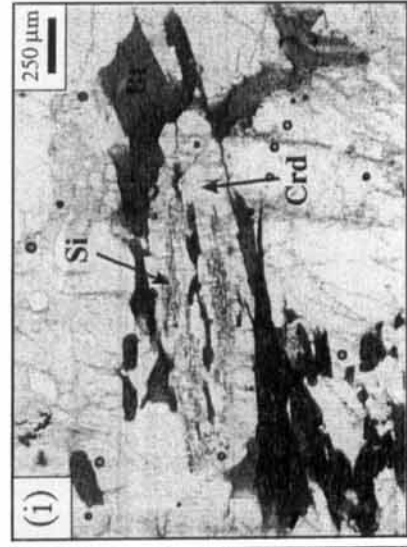
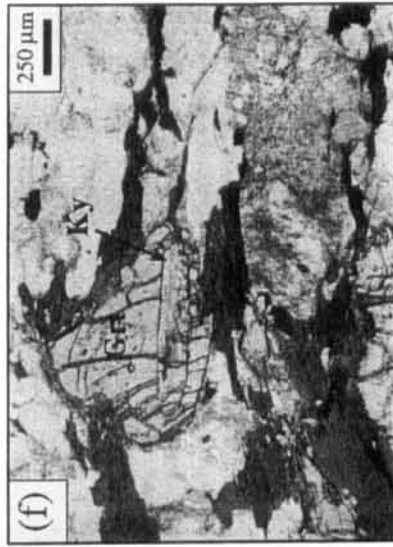


**Table 1.** Major silicate phases in metapelites from Bhutan\*.

	Pl	Bt	Ms	Grt	Ky	Si	St	Crd	Kfs
<b>High Structural Levels</b>									
87-25	x	x	t,r	x	i	x		x	x
87-26		x		x		x		x	x
87-30	x	x	t,r	x		x		x	x
<b>Low Structural Levels</b>									
93Bh2	x	x	r	x		f,i	x,i		
87-6	x	x	x	x		f	x		
93Bs27	x	x	x	x			x		
93Bp100	x	x	x	x	x		x		
93Bp92a	x	x	x	x					
93Bp96a&b	x	x	x	x	x	f			
93Bs42	x	x	x	x	x	f			
93Bs43	x	x	x	x					

\* All samples contain quartz; t=trace, r=retrograde, i=inclusion in garnet, f=fibrolitic sillimanite. Mineral abbreviations from Kretz (1983).

Reaction textures are summarized in Table 2 and illustrated in Fig. 2. Quantitative X-ray maps of garnet from some of the samples in Fig. 2 are shown in Fig. 3. These maps are discussed in a subsequent section. Thin sections were cut perpendicular to the foliation and parallel to the stretching lineation. Reactions (4), (6) and (8) were also described by Swapp & Hollister (1991).

**Table 2.** Metamorphic reaction textures in metapelites from Bhutan.

Reaction	Texture (Fig. 2)	Garnet Composition (Fig. 3)
(1) Ms + Grt + fluid → St + Bt + Qtz 93Bp100	—Bt in pressure shadows between Grt and Ms (Figs 2d & 3c) —subhedral St along Grt rims	—rims depleted in MgO; pronounced when in contact with Bt (Fig. 3c) —rims enriched in MnO —CaO zoning irregular with apparent truncations at margins
(2) St + Qtz → Sil + Grt + fluid 93Bh2	—St and St + Sil inclusions in Grt (Fig. 2e) —corroded St in matrix of Sil–Grt schists	
(3) St + Qtz → Ky + Grt + fluid near 93Bp100 and 87-25	—intergrowths of Ky and Grt —St inclusions in Grt, and corroded St matrix of Ky–Grt schists	
(4) Ky → Sil near 93Bp100 and 87-25	—fibrolitic sillimanite partially replacing bent and broken Ky —fibrolitic sillimanite in matrix of Ky–Grt schists —Ky inclusions in Grt in Sil–Grt schists (Figs 2f & g)	
(5) Grt + Ms → Bt + Sil + Qtz 93Bp96 and 93Bp42	—Bt + Sil growing in Grt pressure shadows (Fig. 2b) —Bt growing in pressure shadows between Grt and Ms (Figs 2h & 3d); Sil in matrix	—CaO zoning irregular —rims enriched in FeO/(FeO + MgO) except where in contact with biotite (Fig. 3d)
(6) Ms + Qtz → Sil + Kfs + fluid(melt?) 87-25	—coarse-grained Sil and abundant Kfs —no muscovite —migmatitic texture	
(7) Bt + Sil + Qtz → Crd + Kfs + fluid 87-30	—Crd + Kfs partially replacing Bt and Sil (Fig. 2i)	
(8) Grt + Sil + Qtz + fluid → Crd 87-26	—Crd partially replacing Grt (Fig. 3e)	—irregular enrichment in FeO/(FeO + MgO) at rims (Fig. 3e) —Crd rims enriched in MgO at Grt contacts

Note: example sample locations from Fig. 1 are given below each reaction in column 1.

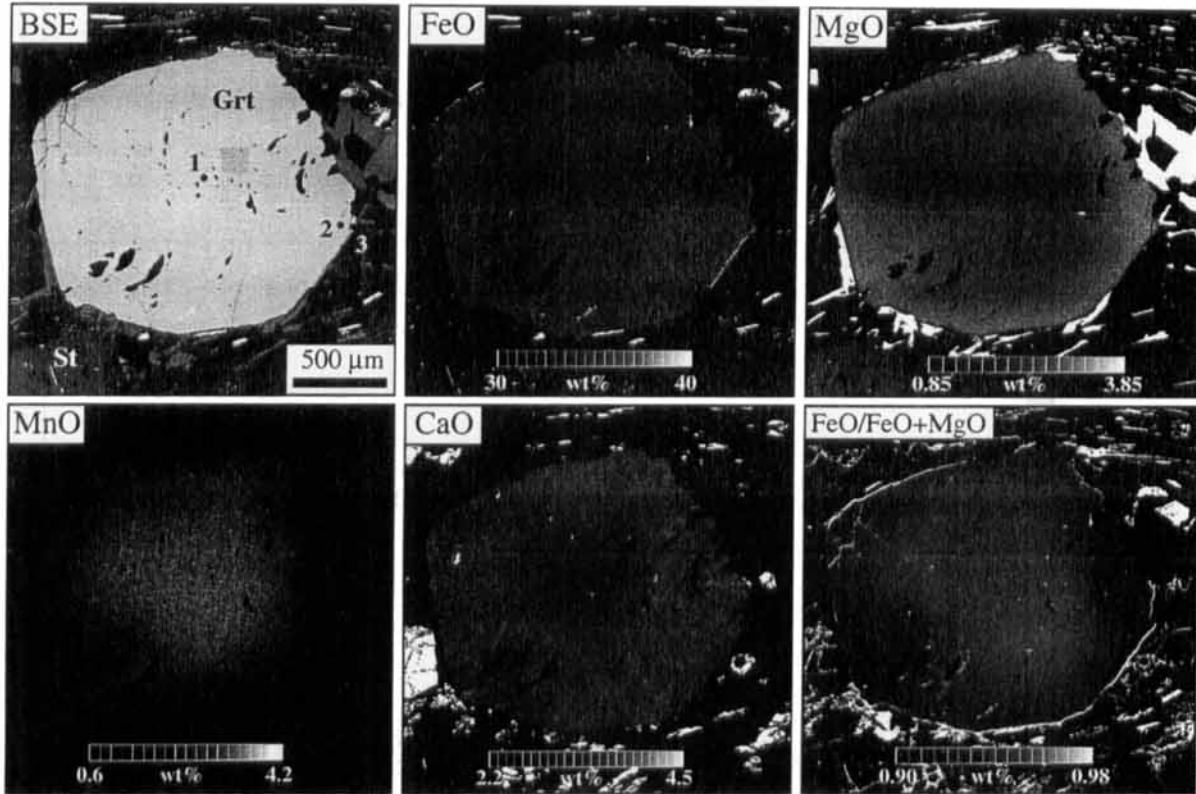
### A petrogenetic grid for Bhutan

Based on the reactions described in Table 2 and illustrated in Fig. 2, a petrogenetic grid for the HHC of Bhutan was constructed. This grid is constructed in the KFMASH system (Fig. 4), based on the thermodynamic database of Berman (1988) with revisions until June, 1992; the computer program PTAX (Berman, 1991) was used for many of the calculations. Garnet, biotite, staurolite and cordierite are assumed to be solid solutions between their respective Fe and Mg end-members; the rest of the solid phases are assumed to be pure. The grid was calculated for partial pressures of H<sub>2</sub>O of 1.0 and 0.7 in the fluid phase.

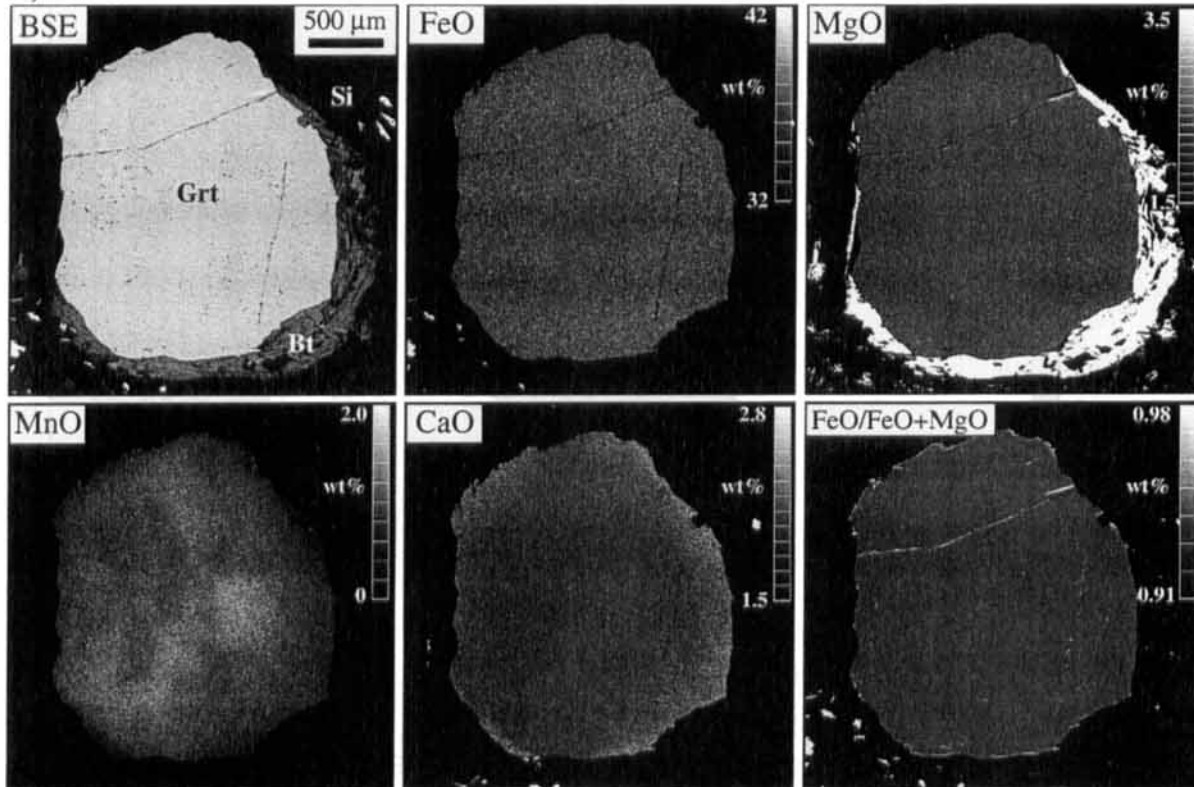
The position of reaction (6) is unaffected by solid solution. The positions of reactions (2) and (3) were calculated using the Fe end-members because solid solution shifts these reactions very little (Ganguly, 1972; Pigage, 1976; Lang & Rice, 1985). Invariant points A and B (Fig. 4a) were fixed by the intersection of reaction (5) and reactions (2) and (6). The position of reaction (5) is affected by solid solution; therefore, we have calculated the position of this reaction for different garnet and biotite compositions (Fig. 5). For each isopleth in Fig. 5, the garnet composition was

**Fig. 3.** Quantitative X-ray maps and backscattered electron images of garnet from Bhutan. A colour version of this figure is accessible via the JMG home page on the World Wide Web at <http://www.gly.bris.ac.uk/www/jmg/jmg.html> and at the equivalent URLs of the Australian and USA sites. The zoning patterns discussed in the text are based on these colour figures, which are superior to the greyscale reproduction of this figure, which masks most of the subtle zoning present in these garnet grains. The scale bar is for weight per cent of the oxide, which is optimized to show zoning in garnet. Weight per cents that lie below and above the scale-bar limits are black and white (purple and red in the colour figures), respectively. Weight per cents were calculated from X-ray intensities assuming a linear relationship between intensity and measured compositions; images using mole per cents would look the same. Black points on the BSE images show locations of microprobe analyses given in Table 3(a).

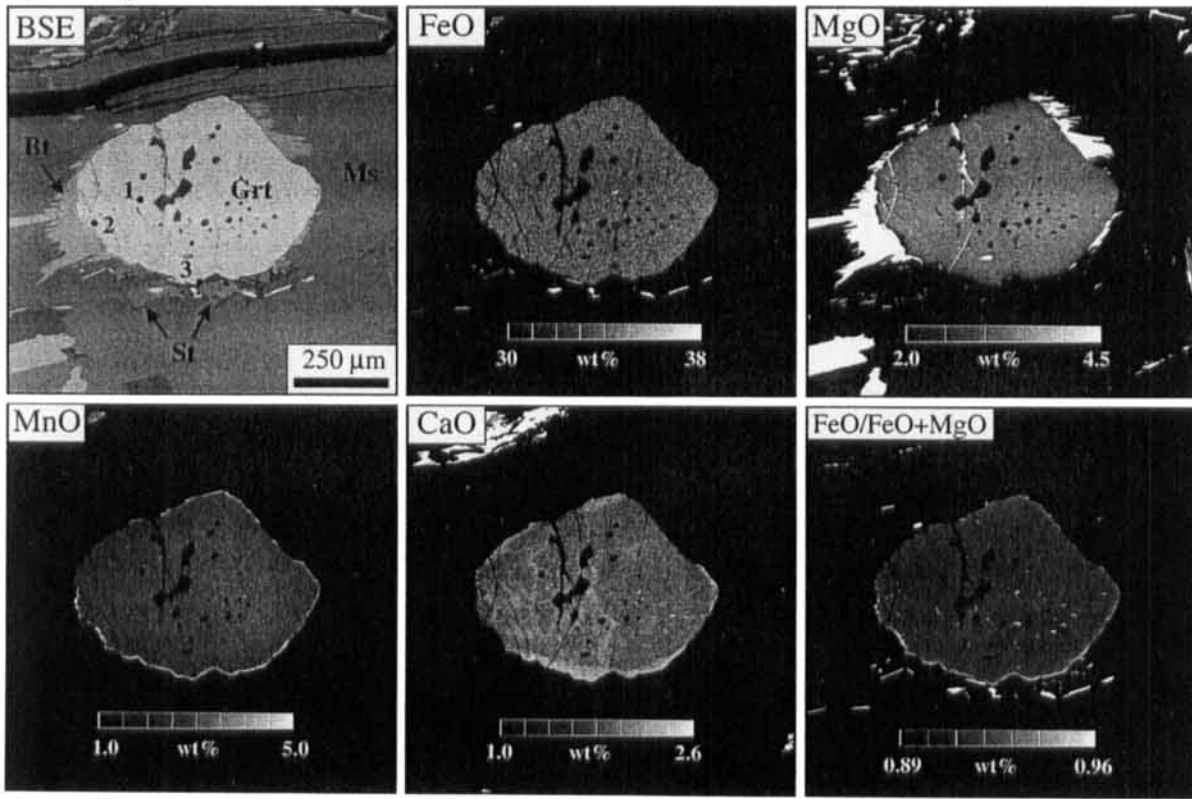
a) 93Bs27



b) 87-6



c) 93Bp100



d) 93Bs42

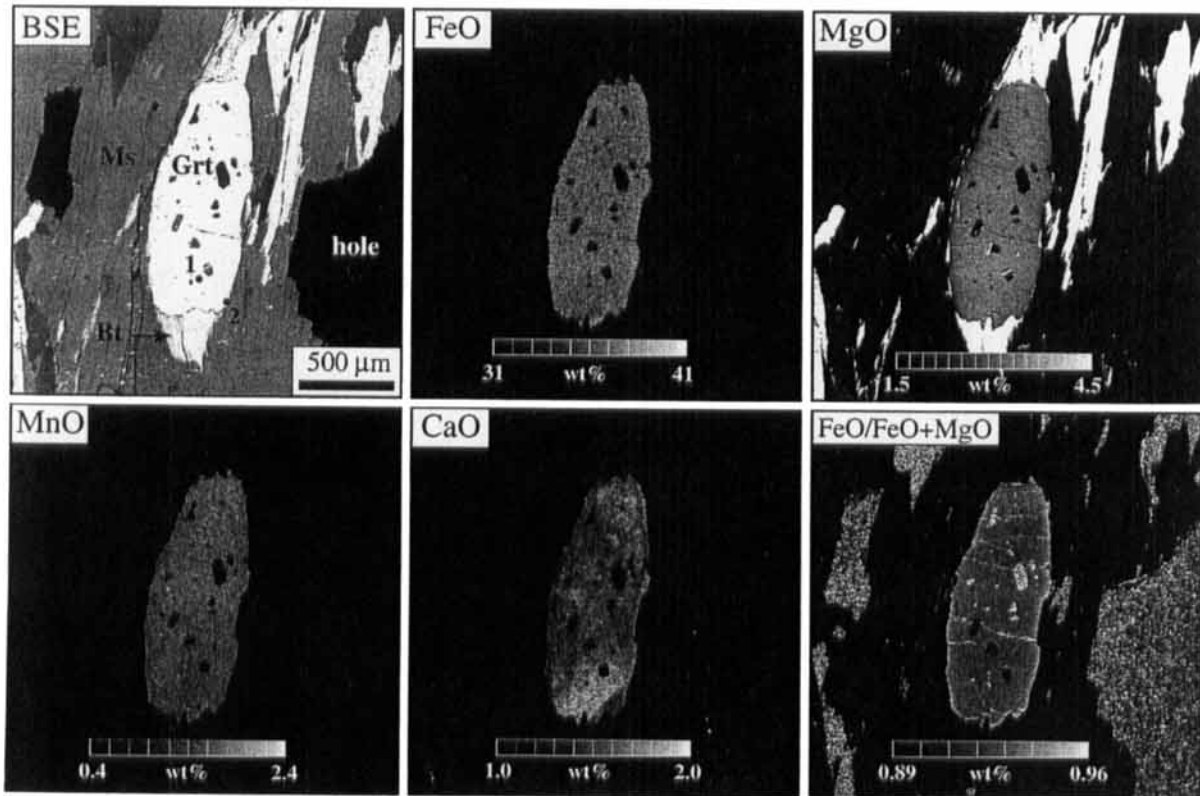
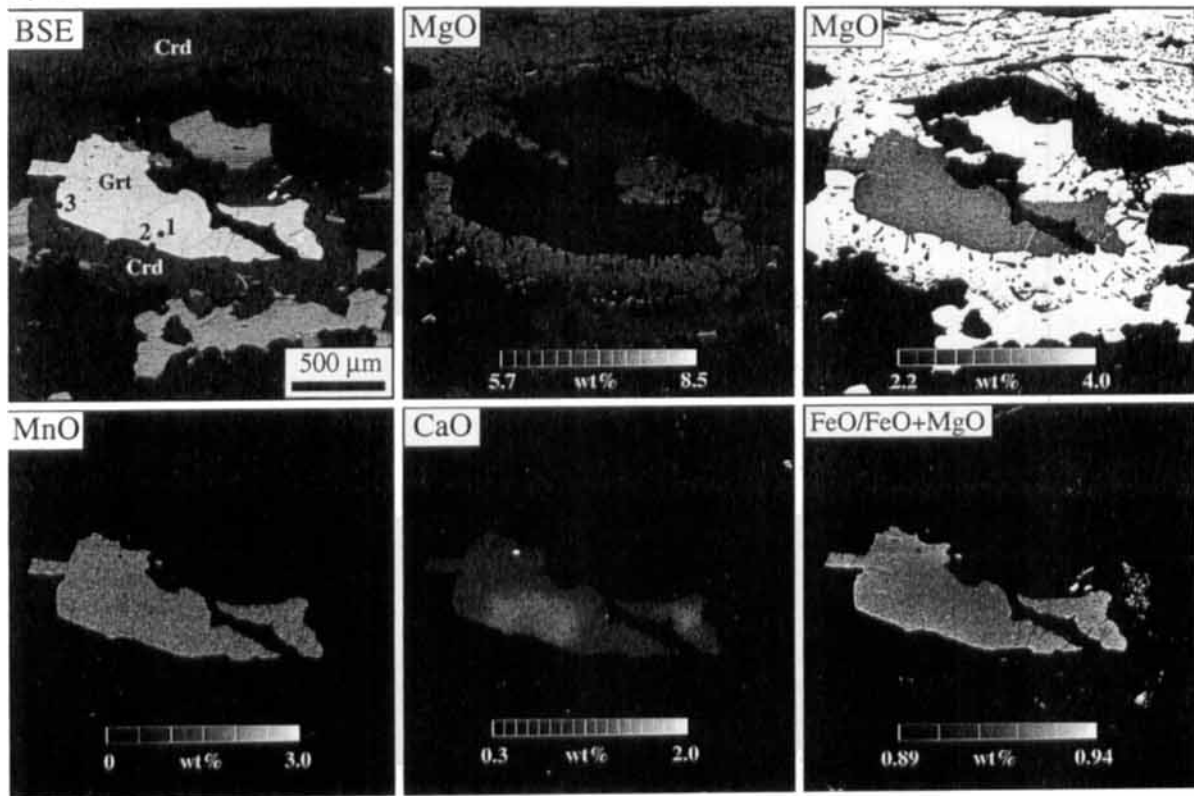


Fig. 3. (continued).

e) 87-26



f) 93Bs43

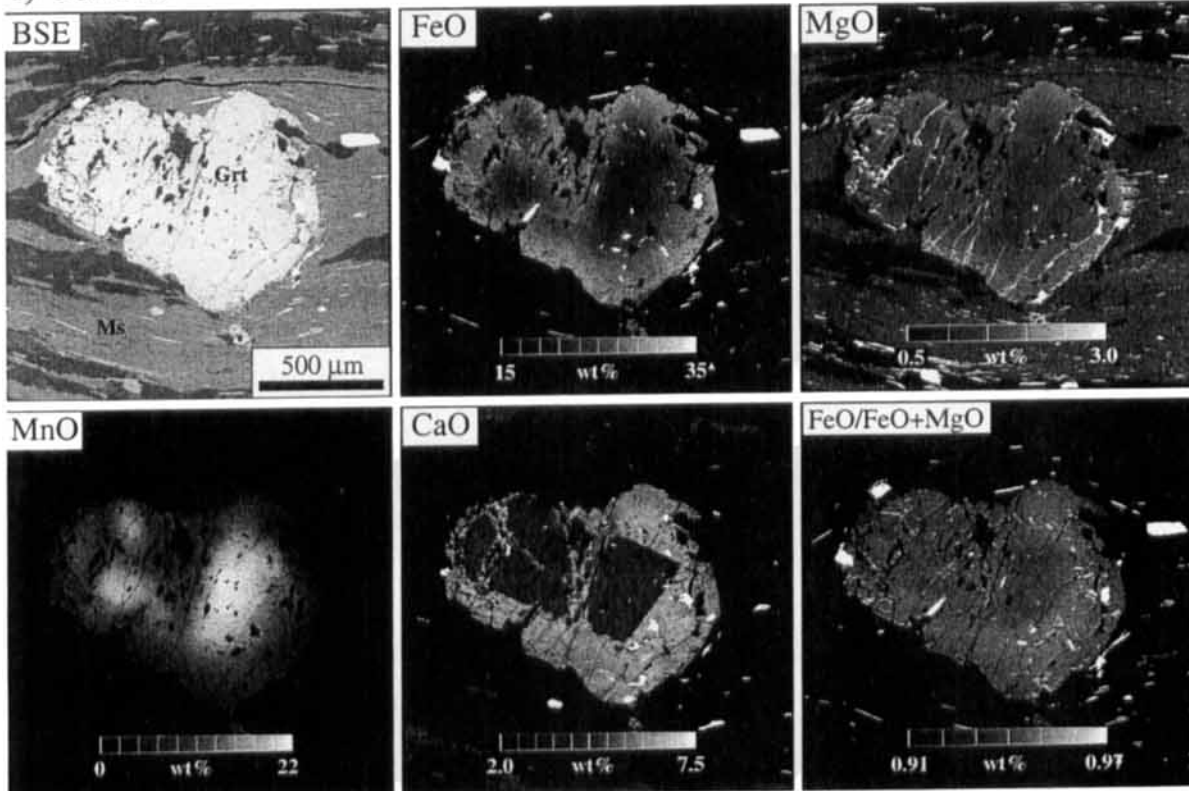


Fig. 3. (continued).

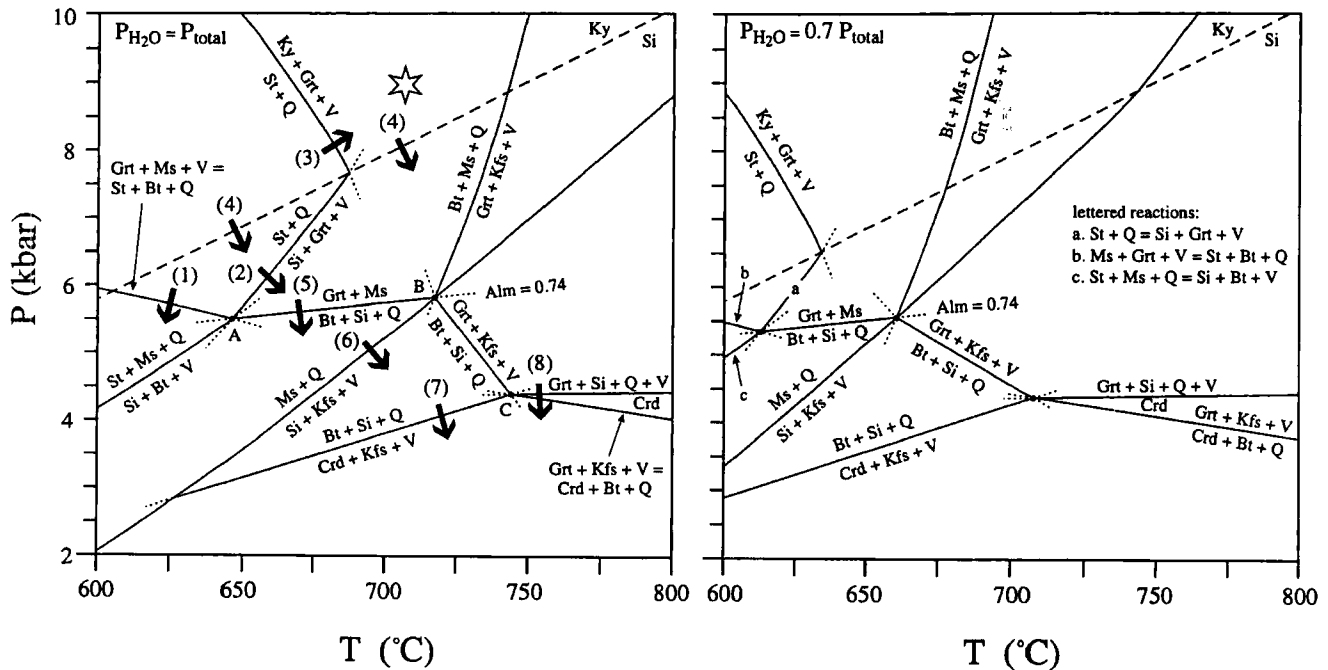


Fig. 4. Petrogenetic grids ( $P_{\text{H}_2\text{O}} = P_{\text{total}}$  and  $P_{\text{H}_2\text{O}} = 0.7 \times P_{\text{total}}$ ) for metapelites from Bhutan. Mineral abbreviations from Kretz (1983) and V = vapour phase. Thick numbered arrows show the direction different rocks from the HHC crossed a reaction line as inferred from the reaction textures described in Table 2. Note that, with the exception of reaction (3), all the arrows show a decompression  $P$ - $T$  path for these rocks. The star shows the approximate peak metamorphic conditions recorded by kyanite-bearing migmatites near Tashigang (Fig. 1).

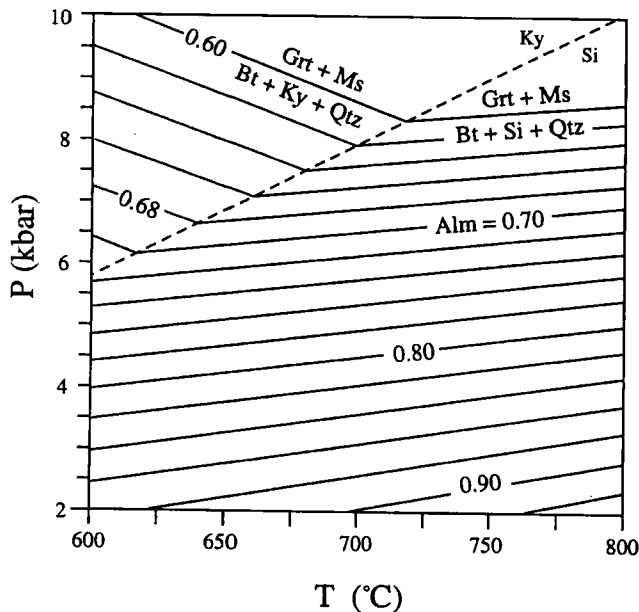


Fig. 5. Garnet isopleths for reaction (5). Biotite compositions calculated using the Ferry & Spear (1978) geothermometer; all other phases are assumed to be pure. The  $\text{Alm} = 0.74$  isopleth was used to construct Fig. 4 (see text).

fixed and the biotite composition calculated at 600 and 800 °C using the Ferry & Spear (1978) geothermometer. The effect of non-KFMASH components on this equilibrium was not considered in our calculations;

however, because these components are minor (e.g. sample 93Bp100, Table 3), their presence probably does not significantly change the position or slope of this reaction. A garnet composition of  $X_{\text{Fe}} = 0.74$  was chosen to plot on the grid in Fig. 4. This is a typical value for almandine garnet such as those found in Bhutan (Table 3a; also see Swapp & Hollister, 1991).

Invariant point C was fixed from the intersection of reactions (7) and (8). The slopes of these reactions were calculated for fixed compositions of cordierite, biotite and garnet (Table 4). Note that these reactions are continuous; as the reactions proceed (for example during decompression), the compositions of cordierite and garnet (or biotite) change. This is clearly seen in sample 87-26, where cordierite in the matrix and that farthest away from garnet, in the cordierite halo around garnet, have MgO values more than 1 (absolute) weight per cent lower than those immediately adjacent to garnet (Fig. 3e). A corresponding decrease in weight per cent MgO of the garnet occurs towards the garnet rim. Because garnet core and matrix cordierite compositions are relatively uniform (Fig. 3e), it was assumed that these compositions more closely reflect equilibrium before decompression and cooling of these rocks. Therefore, garnet core and matrix cordierite compositions (Table 4) were used to calculate the position of reaction (8) in Fig. 4. However, if garnet and cordierite compositions from next to the garnet rim were used (Table 4), reaction (8) plots about 800 bar below the curve shown on the grid (at

**Table 3a.** Selected garnet analyses.

sample:	87-26			93Bs27			93Bp100			93Bs42	
	1	2	3	1	2	3	1	2	3	1	2
SiO <sub>2</sub>	37.86	37.27	37.78	37.15	37.79	38.08	37.86	37.77	37.60	36.88	36.84
Al <sub>2</sub> O <sub>3</sub>	21.57	21.21	21.33	21.00	21.40	21.28	21.26	21.37	21.13	20.06	20.35
TiO <sub>2</sub>	0.00	0.06	0.02	n.d.	n.d.	n.d.	0.00	0.00	0.01	0.00	0.03
FeO	36.31	36.54	37.27	34.18	34.01	34.67	33.10	33.64	33.16	36.27	36.46
MgO	3.24	2.72	2.91	2.11	3.10	2.66	3.75	3.69	3.32	3.45	2.94
MnO	1.89	2.00	1.94	2.95	1.37	1.57	1.93	1.72	1.95	1.32	1.40
CaO	1.32	1.09	0.97	2.74	3.25	2.82	2.02	2.17	2.33	1.62	1.34
K <sub>2</sub> O	0.00	0.02	0.01	n.d.	n.d.	n.d.	0.00	0.01	0.02	0.00	0.01
Na <sub>2</sub> O	0.02	0.00	0.00	n.d.	n.d.	n.d.	0.07	0.05	0.11	0.03	0.03
total:	102.20	100.90	102.23	100.12	100.92	101.05	99.98	100.42	99.62	99.63	99.39
<i>Cations based on 12 oxygens:</i>											
Si	2.99	2.99	2.99	3.00	3.00	3.02	3.02	3.01	3.02	3.00	3.00
Al	2.01	2.01	1.99	2.00	2.00	1.99	2.00	2.01	2.00	1.92	1.96
Ti	0.00	0.00	0.00	0.00	0.00	0.00	0.00	0.00	0.00	0.00	0.00
Fe <sup>2+</sup>	2.40	2.45	2.47	2.31	2.26	2.30	2.21	2.24	2.23	2.47	2.49
Mg	0.38	0.33	0.34	0.25	0.37	0.31	0.45	0.44	0.40	0.42	0.36
Mn	0.13	0.14	0.13	0.20	0.09	0.11	0.13	0.12	0.13	0.09	0.10
Ca	0.11	0.09	0.08	0.24	0.28	0.24	0.17	0.19	0.20	0.14	0.12
K	0.00	0.00	0.00	0.00	0.00	0.00	0.00	0.00	0.00	0.00	0.00
Na	0.00	0.00	0.00	0.00	0.00	0.00	0.01	0.01	0.02	0.00	0.00
total:	8.01	8.01	8.01	8.00	8.00	7.98	7.99	8.00	7.99	8.04	8.02
X <sub>Fe</sub>	0.80	0.82	0.82	0.77	0.75	0.78	0.75	0.75	0.75	0.79	0.81
X <sub>Mg</sub>	0.13	0.11	0.11	0.08	0.12	0.11	0.15	0.15	0.13	0.13	0.12
X <sub>Mn</sub>	0.04	0.05	0.04	0.07	0.03	0.04	0.04	0.04	0.05	0.03	0.03
X <sub>Ca</sub>	0.04	0.03	0.03	0.08	0.09	0.08	0.06	0.06	0.07	0.05	0.04
Fe/(Fe + Mg)	0.86	0.88	0.88	0.90	0.86	0.88	0.83	0.84	0.85	0.86	0.87
T (°C)	749	676	694	491	606	550	815	749	712	705	644

\*T calculated at 6 kbar using garnet mixing model of Berman (1990) and biotite mixing model of McMullin *et al.* (1991). Biotite compositions taken from Table 3(b). See Fig. 3 for analysis locations; n.d. = not determined.

**Table 3b.** Representative matrix biotite analyses.

Sample:	87-26	93Bs27	93Bp100	93Bp96	93Bs42
SiO <sub>2</sub>	35.37	36.05	35.96	35.74	34.88
Al <sub>2</sub> O <sub>3</sub>	18.39	19.56	19.07	18.77	18.83
TiO <sub>2</sub>	5.57	1.92	1.26	1.54	2.67
FeO	21.45	18.75	20.75	20.37	21.10
MgO	6.57	10.14	8.77	9.52	8.24
MnO	0.03	0.03	0.11	0.05	0.00
CaO	0.05	0.00	0.00	0.00	0.02
K <sub>2</sub> O	9.17	8.49	8.99	9.04	8.76
Na <sub>2</sub> O	0.26	0.26	0.33	0.45	0.45
total:	96.85	95.20	95.23	95.48	94.96
<i>Cations based on 11 oxygens:</i>					
Si	2.67	2.72	2.75	2.72	2.68
Al <sup>iv</sup>	1.33	1.29	1.26	1.30	1.32
Al <sup>vi</sup>	0.31	0.45	0.46	0.41	0.39
Ti	0.32	0.11	0.07	0.09	0.15
Fe <sup>2+</sup>	1.36	1.18	1.33	1.30	1.36
Mg	0.74	1.14	1.00	1.08	0.94
Mn	0.00	0.00	0.01	0.00	0.00
Ca	0.00	0.00	0.00	0.00	0.00
K	0.88	0.82	0.88	0.88	0.86
Na	0.04	0.04	0.05	0.07	0.07

a given temperature). The positions of the remaining reactions are fixed by the invariant points. Finally, the star in Fig. 4 shows the approximate peak metamorphic conditions recorded by kyanite-bearing migmatites near Tashigang (Fig. 1); this assumes that kyanite and melt are in equilibrium.

**Table 4.** Microprobe analyses used to calculate reactions (7) & (8) in Fig. 4.

	Reaction (7)		Reaction (8)			
	Crd	Bt	Grt (core)	Grt (rim)	Crd (ng)*	Crd (ag)*
SiO <sub>2</sub>	49.78	35.38	37.86	37.27	48.91	48.65
Al <sub>2</sub> O <sub>3</sub>	32.95	18.99	21.57	21.21	33.22	33.21
TiO <sub>2</sub>	-	4.34	0.00	0.06	0.04	0.06
FeO	8.19	17.62	36.31	36.54	9.87	10.50
MgO	7.99	8.90	3.24	2.72	7.28	6.99
MnO	0.35	0.16	1.89	2.00	0.13	0.16
CaO	0.03	0.02	1.32	1.09	0.02	0.05
K <sub>2</sub> O	-	9.28	0.00	0.02	0.02	0.01
Na <sub>2</sub> O	0.11	0.15	0.02	0.00	0.20	0.19
total:	99.40	94.84	102.20	100.90	99.67	99.81
<i>Cations based on:</i>						
	18 ox.	11 ox.	12 ox.	12 ox.	18 ox.	18 ox.
Si	4.97	2.68	2.99	2.99	5.00	4.98
Al	4.04	1.70	2.01	2.01	4.01	4.01
Ti	-	0.25	0.00	0.00	0.00	0.01
Fe <sup>2+</sup>	0.71	1.12	2.40	2.45	0.84	0.90
Mg	1.24	1.01	0.38	0.33	1.11	1.07
Mn	0.03	0.01	0.13	0.14	0.01	0.01
Ca	0.00	0.00	0.11	0.09	0.00	0.01
K	-	0.90	0.00	0.00	0.00	0.00
Na	0.02	0.02	0.00	0.00	0.04	0.04
total:	11.01	7.69	8.01	8.01	11.02	11.03

Note: reaction (7) compositions from sample 87-30 (Swapp & Hollister, 1991); reaction (8) compositions from sample 87-26 (this study). \*ng = next to garnet; ag = away from garnet.

### Mineral zoning: implications for geothermobarometry

Many of the samples discussed above have appropriate mineral assemblages for geothermobarometry, for example garnet, biotite, muscovite, plagioclase, quartz,  $\pm$  sillimanite and/or kyanite (Table 1). These phases can be adequately represented by the KCaFMASH system, which, when combined with the above phases, gives three independent reactions [e.g. the garnet–biotite Fe–Mg exchange geothermometer (Ferry & Spear, 1978), the GASP geobarometer (Ghent, 1976) and the GMPB (Ghent & Stout, 1981) geobarometer]. However, to apply these geothermobarometers, it must be assumed that all of these phases were in equilibrium and that, after equilibrium was achieved, the equilibrium compositions were preserved, or can be inferred from measured compositions. Berman (1991) suggested a quantitative way to check for equilibrium in rocks for which more than two independent reactions can be written: calculate all possible reactions (stable and metastable) for the rock and see if they intersect within a small region of  $P$ – $T$  space. If they do, then the phases used for the calculation might have been in equilibrium. This is a good test for rocks with three or more independent equilibria; however, it is more common to have only two independent reactions, which is the case for most of the Bhutan samples.

An alternative approach for testing for equilibrium in a rock is to test for homogeneity of phase compositions. For refractory phases such as garnet, it is commonly assumed that the garnet rim was in equilibrium with the matrix phases. This will be true for rocks where garnet and the rest of the phases in the rock achieved equilibrium, and did not continue to exchange cations during cooling or experience subsequent net-transfer reactions involving the consumption of garnet.

### Quantitative X-ray maps

The wealth of reaction textures preserved in the Bhutan rocks show that many of these rocks experienced net-transfer reactions during decompression. That is, almost all of the reactions described in the previous section were crossed in the direction of decompression. This suggests that many of these rocks may not preserve phase compositions that reflect the peak metamorphic conditions experienced by these rocks. To test this, quantitative X-ray images of garnet and the surrounding matrix minerals (Fig. 3) were acquired.

A first-order approximation for the maximum metamorphic temperature a rock experienced may be obtained by examining garnet zoning patterns (Yardley, 1977; see Tracy, 1982, for a review). In many of the rocks from the HHC of Bhutan, garnet has irregular zoning of CaO, is relatively unzoned in MnO and FeO, and is typically depleted in MgO near the rim (e.g. 93Bs42, Fig. 3d). This type of zoning pattern

suggests that these rocks experienced temperatures of over 600–650 °C for a period of time long enough that intracrystalline diffusion mostly homogenized the internal composition of the garnet (Woodsworth, 1977; references in Tracy, 1982). The MgO depletion [and increase in  $\text{FeO}/(\text{FeO} + \text{MgO})$ ] near the rim is typically attributed to cation exchange between garnet and the matrix during cooling (e.g. Tracy *et al.*, 1976; Spear, 1991). The plot of  $\text{FeO}/(\text{FeO} + \text{MgO})$  is included for all of the samples in Fig. 3 because it can be used as a proxy for temperature, where higher values of  $\text{FeO}/(\text{FeO} + \text{MgO})$  correspond to lower temperatures.

An example of a growth-zoned garnet is shown in Fig. 3(a). This garnet staurolite schist from below the Kakhtang thrust (93Bs27, Fig. 1) is one of the lowest-grade rocks found in the HHC of Bhutan. In this garnet, MnO decreases, CaO and MgO increase, and FeO is relatively constant from core to rim. This zoning pattern suggests that this garnet grew during prograde metamorphism (Hollister, 1966; Tracy *et al.*, 1976), and that the garnet never reached temperatures high enough for diffusion to internally homogenize it (Woodsworth, 1977). However, there is a slight increase in  $\text{FeO}/(\text{FeO} + \text{MgO})$  at the rim, which suggests that there was incipient exchange between garnet and the matrix as the rock cooled. The increase in CaO from core to rim might indicate that this garnet grew under increasing pressure conditions, or marks a change in the reaction history of the rock involving a Ca-rich phase such as plagioclase (Crawford, 1974).

The presence of spiral inclusion trails in garnet and staurolite from these rocks (Figs 2a & 3a) shows that these phases grew during deformation. This implies that this part of the HHC of Bhutan was being deformed during prograde heating.

Garnet zoning in the nearby garnet sillimanite schists, such as 87–6 (Figs 1 & 3b), contrasts sharply with that in the garnet staurolite schists. In these higher-grade rocks, garnet is corroded and surrounded by mats of sillimanite and biotite. In the garnet shown in Fig. 3(b), FeO and MgO are constant from core to rim. MnO is irregularly zoned from patchy higher concentrations near the core to lower concentrations at the rim. In general, CaO increases towards the rim, but the CaO-rich rim is irregular and appears to be truncated. This type of irregular CaO zoning is typical in most of the rocks from the HHC (Fig. 3c–e).  $\text{FeO}/(\text{FeO} + \text{MgO})$ -enriched rims are also common in these rocks (e.g. Fig. 3c–e), and MnO-enriched rims are present in some of the samples (e.g. Fig. 3c). These zoning patterns suggest that garnet in most of these rocks has been partially resorbed and is not in equilibrium with the matrix minerals.

A garnet from a garnet–muscovite schist of the Lesser Himalaya has a very different zoning pattern from the typical garnet zoning patterns in the HHC (93Bs43, Fig. 3f). It is strongly zoned in FeO, MgO, MnO and CaO, and has a distinct low-CaO euhedral core surrounded by a high-CaO rim. A remarkable aspect

to the zoning in this garnet is the differences in apparent mobility between the different cations suggested by the element distribution patterns. CaO retains a sharp boundary between the euhedral core and the CaO-rich rim, whereas diffusion appears to have smoothed this boundary to different degrees for FeO, MgO and MnO. This suggests that this rock experienced temperatures high enough for FeO, MgO and MnO to partially diffuse, but not high enough for CaO to be mobile (see also Woodsworth, 1977; Yardley, 1977; Loomis, 1978).

#### Discussion of the metamorphic reaction microstructures and garnet zoning

The most striking aspect of the reactions identified in the HHC of Bhutan is that all, with the exception of reaction (3), are decompression and/or heating reactions. Each short bold arrow shown in Fig. 4(a) represents one possible  $P$ - $T$  path for the rock, which contains the reaction number attached to the arrow. The arrows are arbitrarily drawn normal to the reaction curves. Because of the low slopes of many of these reactions, the simplest explanation for the formation of the set of reaction microstructures observed in all these rocks is that they formed during nearly isothermal decompression, but perhaps with some heating.

Another striking feature of these reactions, when considered together, is that they occur over a range of temperatures. That is, reaction (1) occurs at temperatures about 100 °C less than reaction (8) (the temperature difference between invariant points A and C in Fig. 4a&b). This implies that temperature did not continually increase with depth within the HHC of Bhutan at the time of decompression. For example, some of the lowest-grade rocks in the HHC (sample 93Bs27) occur beneath the Kakhtang thrust, in the structural middle of the HHC (Fig. 1). These lower-grade garnet-staurolite schists have garnet zoning patterns (Fig. 3a) that indicate that these rocks were never above 600–650 °C, or at least not for any significant length of time (as discussed above). These rocks contrast markedly with the sillimanite-bearing and migmatitic rocks that occur structurally above and below these low-grade rocks.

Along strike from the garnet-staurolite schists (i.e. 93Bs27), and at approximately the same structural level (i.e. 93Bh2 and 87-6, see Fig. 1), sillimanite appears and staurolite gradually disappears due to reaction (2) and possibly (5), or more likely by a more complicated reaction path similar to that proposed by Swapp & Hollister (1991), namely biotite + muscovite + staurolite + quartz  $\rightarrow$  sillimanite + higher Fe/Mg biotite + higher Fe/Mg staurolite + garnet + higher Na/Ca plagioclase + H<sub>2</sub>O. Garnet zoning in these higher-grade rocks (e.g. 87-6, Fig. 3b) suggests that these rocks were at high enough temperatures (> 600–650 °C) for a long enough period of time for intracrystalline diffusion to homogenize the com-

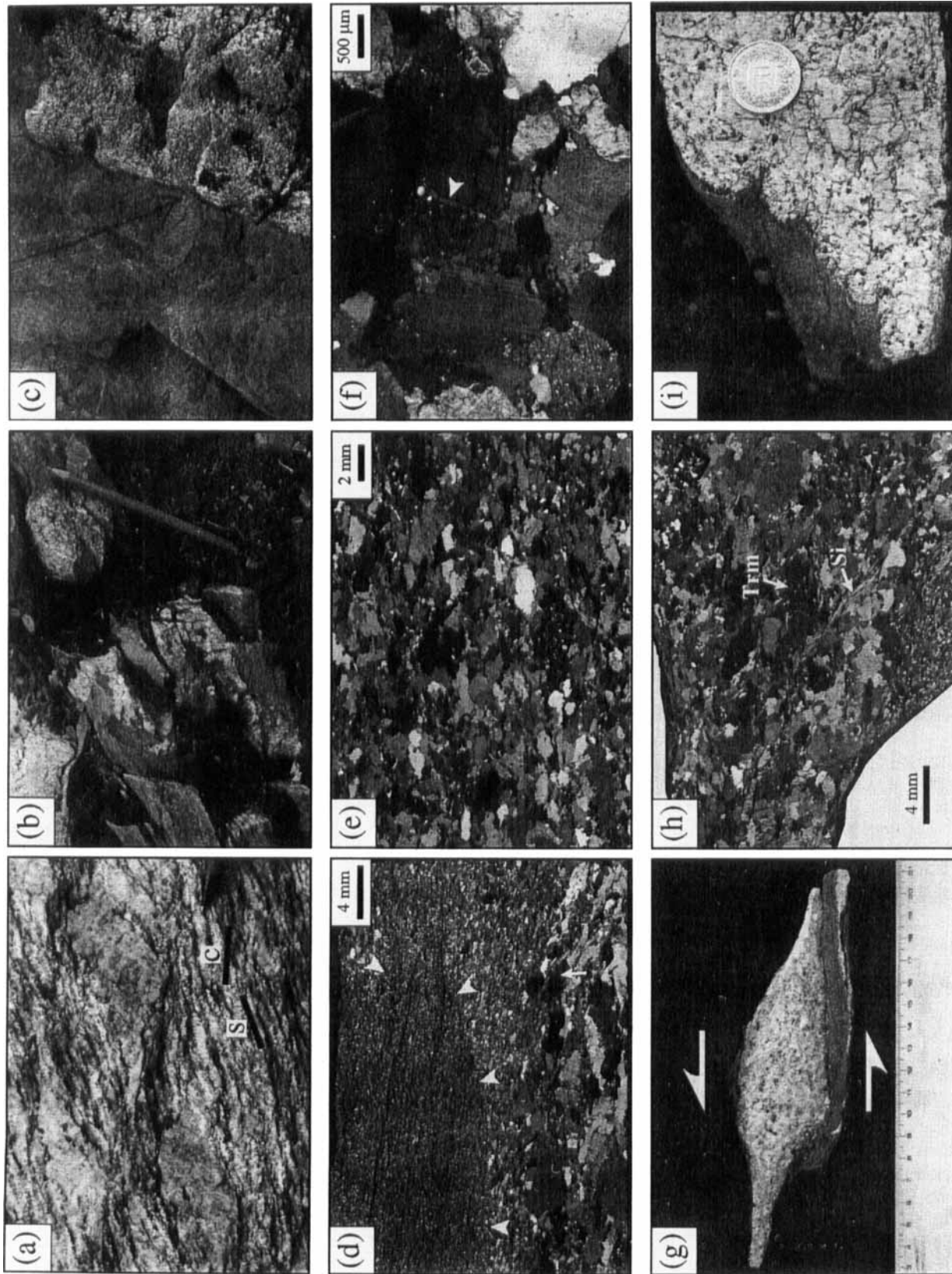
position. Therefore, even within the same structural level of the HHC, there were large differences in temperature at the time of decompression, assuming that no major post-decompression faults are present. This is in marked contrast to areas west of Bhutan, such as in Nepal and India, where, based on geothermometry, temperatures are interpreted to have been nearly uniform across the HHC (Hodges *et al.*, 1988a; Pêcher, 1989).

#### SYNKINEMATIC INTRUSION OF LEUCOGRANITE

In the previous section we presented evidence that the HHC of Bhutan experienced decompression while maintaining a laterally heterogeneous and locally inverted internal temperature distribution. Below, evidence is presented for intrusion of leucogranite dykes and sills into the HHC during this exhumation, and it is suggested that intrusion of the leucogranites provided some of the extra heat to locally vary the temperature.

Most of the rocks in the HHC of Bhutan have well-developed foliations defined by the shape preferred orientation of micas. S-C fabrics, shear-band orientations (Fig. 6a) and quartz textures (Grujic *et al.*, 1996) showed that these rocks experienced top to the south shearing during the main foliation forming event. Leucogranite dykes cut the existing foliation and are folded within it (Fig. 6b-d). On the mesoscopic scale this dyke cross-cuts a pre-existing schistosity and N-S-orientated stretching lineation in the country rock. In Fig. 6c, the dyke truncates the pre-existing stretching lineation in the country rocks, and no macroscopic lineation is visible in the dyke, yet, it is also tightly folded with fold axial planes parallel to the same foliation in the country rock. On the microscopic scale, in the middle of the dyke, many features of the magmatic fabric are preserved with a weak solid-state overprint. For example, near the contact with the country rocks, plagioclase and quartz in the dyke are finer grained and have been dynamically recrystallized (Fig. 6d). In profile view, the axial-plane schistosity passes continuously from the country rock into the dyke, with cleavage refraction indicating relatively more competent behaviour of the dyke. These relationships indicate that, although the dyke was intruded after the development of a substantial part of the total strain, it was tightly folded and deformed in the magmatic and subsequently the solid state during progressive deformation.

Leucogranite sills up to 600 m thick are also present throughout the HHC of Bhutan. These sills tend to have well-developed magmatic and submagmatic foliations (submagmatic flow implying solid-state deformation of crystals in the presence of melt), with minor amounts of solid-state overprinting (Fig. 6e). Some of this solid-state deformation took place at temperatures near the solidus and hence immediately following leucogranite intrusion, as indicated by prism <c> slip



in a quartzite enclosed in leucogranite (Grujic *et al.*, 1996). In some samples, albite-rich plagioclase fills fractures in more anorthite-rich plagioclase crystals (Fig. 6f). These fractures are restricted to single crystals (i.e. they are not through-going fractures) and are typical in rocks that were deformed in the submagmatic state (Bouchez *et al.*, 1992; John & Blundy, 1993; Davidson *et al.*, 1996). Some of the small sills have also been asymmetrically boudinaged, the sigma clast shape of some fragments indicating top to the south shearing (Fig. 6g). In the leucogranite boudin shown in Fig. 6(g), plagioclase and tourmaline have a shape preferred orientation which runs parallel to the boudin walls (Fig. 6h). Sillimanite, probably pulled from the contact with the country rocks, is also aligned with this shape preferred orientation. Quartz in this rock shows straight extinction, and plagioclase appears to have experienced only minor amounts of dynamic recrystallization along its margins. These microstructures suggest that this rock was deformed shortly after intrusion and at very high temperatures, probably while the sill was still partially molten, in order to orientate the large tourmaline and plagioclase phenocrysts without internal deformation of the phenocrysts or the matrix. Some deformation continued in the solid state, but at temperatures high enough to allow for the dynamic recrystallization of plagioclase (> 500 °C; Fitz Gerald & Stünitz, 1993).

Features such as cusped-lobate structures seen along the margins of some of the dykes and sills (Fig. 6i) show that the ambient temperature in the country rock was high enough for the country rocks to have a lower viscosity than the leucogranite during, or shortly after, the solidification of the leucogranite. High temperatures at the time of intrusion of the synkinematic leucogranites are supported by the presence of the synkinematic, prograde garnet staurolite schists in the footwall of the Kakhtang thrust, which suggest that temperatures at the time of intrusion were at least c. 550 °C. Therefore, top to the south deformation, heating and intrusion of the leucogranites appear to have occurred together in the HHC of Bhutan.

The 1993 Swiss–American expedition did not reach the main leucogranite bodies of the Khula Kangri or Gopu La plutons located in the highest structural levels of the HHC (Fig. 1). Gansser (1983) describes the contacts of these plutons as mostly consisting of

dykes and sills which are locally concordant to the fabric in the country rocks but cross-cut the regional fabric. According to Gansser (1983; p. 119), there is no clear-cut contact between the main body of the plutons and the country rock, but rather the plutons ‘are surrounded by an aureole of dykes and sills which can surpass the volume of the central bodies (plutons)’.

According to Burchfiel *et al.* (1992) and Edwards *et al.* (1996), the sense of shear in the country rocks near the structural top of the HHC in Bhutan is reversed, with younger top down to the north shear fabrics overprinting an older top to the south shear fabric. Burchfiel *et al.* (1992) describe leucogranite dykes and sills that intruded the HHC during the earlier top to the south shearing event. Apparently, leucogranite intrusion, including emplacement of the large plutons, continued during and after the later, top down to the north, shearing phase (Burchfiel *et al.*, 1992; Edwards *et al.*, 1996).

## DISCUSSION OF TECTONIC MODELS

A number of tectonic models for the exhumation of the HHC has been proposed in the literature (e.g. LeFort, 1975; Burchfiel & Royden, 1985; Searle *et al.*, 1988; Swapp & Hollister, 1991; Harris & Massey, 1994; Grujic *et al.*, 1996). Common to all of these models is the importance of rapid south-directed thrusting across the MCT (or more distributed shear across a MCTZ, see below). Burchfiel & Royden (1985), drawing on the work of Burg *et al.* (1984), proposed that top down to the north, normal faulting across the South Tibetan detachment system worked in conjunction with thrusting across the MCT, thereby rapidly exhuming the HHC from deep crustal levels by extrusion. Most of these models, however, implicitly assume (1) that the HHC was exhumed as a more or less a rigid body [for example, use of the terms ‘Tibetan Slab’ by LeFort (1975) and others, and ‘crustal wedge’ by Burchfiel & Royden (1985)], and (2) that most of the strain was accommodated across a discrete MCT and South Tibetan detachment system during exhumation.

In some areas, workers have pointed out that the MCT is a broad zone of shear deformation (e.g. Burg & Chen, 1984; Brun *et al.*, 1985). In the Kashmir–Zaskar–Kulu Himalaya, Searle & Rex (1989) defined the MCT as ‘a major ductile shear zone 5–10 km wide,

**Fig. 6.** Structures in the HHC of Bhutan. (a) S–C fabric in orthogneiss basement showing top to the south sense of shear (North is to the left). (b)–(d) Folded leucogranite dyke. Pencil in (b) is approximately 16 cm. (c) View from top of fold (perpendicular to foliation in the country rock) showing lineation in country rock (dark coloured) and lack of a macroscopic lineation in the leucogranite (light coloured). (d) Photomicrograph from the hinge of the fold shown in (b). Arrows show the location of the contact between the leucogranite (coarse-grained material) and the country rock (fine-grained material in upper left). (e) Magmatic fabric in leucogranite sill. (f) Melt (plagioclase)-filled fracture in plagioclase lath in leucogranite (see text for discussion). (g) Leucogranite asymmetric boudin. Major divisions of ruler are in centimetres. (h) Photomicrograph of boudin neck in (g). Note shape preferred orientation of elongate minerals and weak solid-state overprint. (i) Cusped-lobate structure at contact of leucogranite dyke. This shows that the viscosity of the country rocks was lower than that of the leucogranite at the time of (or shortly after) intrusion.

containing several zones of high strain.' Jain & Manickavasagam (1993) argued that the HHC in Jammu and Kashmir 'evolved in a 15–20 km thick, north-east-dipping ductile shear zone.' They implied that the amount of strain was more or less uniform across the HHC, with some localized high-strain zones (see fig. 4b in Jain & Manickavasagam, 1993).

Grujic *et al.* (1996) confirmed this view for the Bhutan Himalaya and proposed the use of the term Main Central Thrust Zone (MCTZ) in order to make a distinction between the wide zone of distributed top to the south shear within the HHC and the MCT, a protolith boundary between the HHC and the Lesser Himalayas (Gansser, 1964). Hence, the MCT is not necessarily a narrow high-strain zone, but rather marks the protolith boundary between the highly strained, penetratively deformed rocks of the HHC and the Lesser Himalayas. This distinction between the MCTZ and the MCT is important because it affects the geometry and boundary conditions for any tectonic model proposed for the exhumation of the HHC.

In addition to the nature of the MCT, there is some controversy over the relationship between the exhumation of the HHC and the generation and emplacement of the leucogranite plutons, which are mostly concentrated within the highest structural levels of the HHC (Harris & Massey, 1994). The two competing (but not mutually exclusive) processes proposed for the generation of the crustally derived leucogranites are: (1) fluid-present melting of the lower hot, dry portions of the HHC due to infiltration of an H<sub>2</sub>O-rich fluid from the dehydrating footwall during thrusting (e.g. LeFort, 1975; Searle *et al.*, 1988); and (2) fluid-absent (decompression) melting in the HHC from the breakdown of muscovite during rapid exhumation (Harris *et al.*, 1993; Harris & Massey, 1994). Experimental work by Scaillet *et al.* (1995) showed that temperatures in the source region of the leucogranites were at least 700 °C, and more likely 750–770 °C. These temperatures suggest that either of these two processes could have generated the leucogranites, but for the case of fluid-present melting, water activities must have been low ( $a_{\text{H}_2\text{O}} \approx 0.5$ ) (Scaillet *et al.*, 1995).

Although both melting processes are possible, the fact that the large leucogranite plutons and the majority of the migmatitic rocks occur in the structurally highest levels of the HHC argues against melting of the base of the HHC due to fluid infiltration from the footwall. Indeed, the migmatitic rocks which occur near the plutons typically lack muscovite and are rich in K-feldspar and sillimanite (e.g. 87-25), suggesting that muscovite reacted out of these rocks (fluid-absent melting) producing K-feldspar, sillimanite and melt (reaction 6 with fluid = melt).

Implicit in most of the *in situ* melting models for the generation of the leucogranites is that melting was *in situ*, with only local transport to form the large plutons. That is, the spatial relationship between the different structural levels within the HHC during

exhumation, melting and emplacement of the leucogranites was largely preserved during exhumation (the concept of the HHC being a rigid slab). However, our work in Bhutan shows that the intrusion of leucogranite dykes and sills occurred during penetrative deformation and top to the south thrusting (Fig. 6). Swapp & Hollister (1991), based on differences in the metamorphic history of rocks in the highest *vs.* the lowest structural levels of the HHC, proposed that the leucogranite plutons and surrounding migmatitic rocks were emplaced by thrusting over the lower structural levels. They proposed the existence of a major thrust fault within the HHC, not identified in the field and named (the Kakhtang thrust) until the Swiss–American expedition in 1993. Based on the observations of the 1996 Bhutan expedition, the Kakhtang thrust fault is an out-of-sequence thrust. Thus, the advection of heat by thrusting and syntectonic migration of the leucogranites up-dip from the root zone of the HHC contributed to the formation of the inverted metamorphic field gradient. Given heat advection from thrusting and contemporaneous leucogranite intrusion, this inverted gradient is very likely to correspond to a situation whereby the isotherms have been temporarily and locally inverted as well.

In contrast, we emphasize that for shearing near the MCT there is no proof that the isotherms were ever inverted at a given time, in spite of the well-documented inversion of the metamorphic field gradient. In-sequence foreland propagation of thrusting may well lead to a situation whereby an inverted metamorphic field gradient is produced by the juxtaposition of material lines connecting points which reached different peak temperatures at different times (e.g. Jamieson *et al.*, 1996).

In the Ladakh–Zaskar region, Searle *et al.* (1988) also proposed a tectonic transport model for the high-grade migmatitic rocks of the HHC. They proposed that the HHC is a crustal-scale fold with some internal shearing, with the fold core containing the high-grade migmatitic rocks originating from the deepest structural levels of the HHC (fig. 18 of Searle *et al.*, 1988). In their model, melting is due principally to fluid infiltration from the footwall of the MCT into the high-grade core of the fold; however, they did not exclude dehydration melting of muscovite and perhaps biotite as alternative sources of melt. Searle *et al.* (1988) also reported leucogranite sills that intruded during south-west-directed thrusting and folding in Ladakh–Zaskar.

The observations in Bhutan (and Ladakh–Zaskar) show that the HHC was intruded by leucogranite during penetrative top to the south thrusting. The contact of the HHC with the overlying Tethyan sedimentary rocks (the STDS) appears to be a relatively narrow zone which accommodated at least 35 km of relative (top down to the north) displacement in the Qomolangma (Everest) area (Burchfiel *et al.*, 1992). The steep metamorphic field gradient across this

contact at La Kang and Gonto La (Fig. 1) (Burchfiel *et al.*, 1992; Edwards *et al.*, 1996), and the presence of a ductile shear zone with top down to the north displacement at Gonto La (Edwards *et al.*, 1996) suggest the presence of a major structural discontinuity in the area of Bhutan as well, but the amount of displacement across this zone has yet to be determined.

The amount of displacement of the basement at the base of the HHC with respect to the basement of the Lesser Himalaya is even less clear than that across the STDS. In Bhutan, the mapped MCT is placed directly below the lowest occurrence of the orthogneisses of the HHC. If these gneisses are reworked Precambrian basement of the Indian Plate, and the metasediments in the footwall of the mapped MCT are the metamorphosed Precambrian and Palaeozoic cover of the same basement (Gansser, 1983), then the MCT must have cut through the cover rocks of the Lesser Himalayas, with the amount of displacement depending on (1) the original thickness of the Palaeozoic cover, and (2) the angle between the MCT and the basement–cover interface. According to Gansser (1983), the lesser Himalaya of Bhutan are ‘geologically complex’ because of sedimentary facies changes and complicated internal structure. The fact that basement (orthogneiss) of the HHC occurs structurally above the metasedimentary cover of the Lesser Himalaya all around the half-window of the Kuru Chu–Shumar spur (near Mongar, Fig. 1), suggests that shearing in the vicinity of the MCT, together with imbrications within the Lesser Himalayan sediments, accommodated a significant amount of displacement, of the order of at least 55 km.

The STDS and the MCT in Fig. 1 thus appear to be important tectonic boundaries in Bhutan that juxtapose the highly sheared, deep-crustal rocks of the HHC between the relatively less deformed and metamorphosed Lesser Himalaya and overlying Tethyan sedimentary rocks (Fig. 7). Large amounts of shearing at the margins of the HHC in combination with top to the south shearing within the lower part of the HHC (MCTZ), associated with local heat advection linked to the intrusion of the leucogranites during exhumation, may explain the range of temperatures recorded by the decompression reactions and garnet zoning patterns. For example, in the area with low-grade rocks below the Kakhtang thrust near 93Bs27, leucogranite dykes and sills are much less common than in the area along strike with higher-grade rocks near 87-6, also located structurally below the Kakhtang thrust (Fig. 1). This confirms that, locally, the leucogranites brought in some heat to help drive reactions and diffusion in garnet. In addition, because the Kakhtang thrust placed hot, migmatitic rocks over lower-grade rocks, and because this inverted metamorphism is preserved, exhumation of the entire HHC must have been rapid after or during the formation of the thrust.

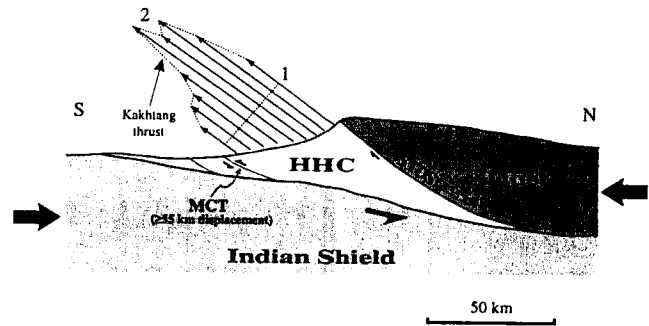


Fig. 7. Tectonic model for the extrusion and exhumation of the HHC of Bhutan (modified from Grujic *et al.*, 1996). The arrows show schematic displacements within the HHC relative to India and Tibet. Displacement differences, due to heterogeneous plastic flow and thrust faulting (e.g. the Kakhtang Thrust), are shown by the change in shape of an imaginary material line for two arbitrarily different times (dashed lines marked by 1 and 2). However, displacements within the HHC are not necessarily synchronous; that is, the higher structural levels may have been extruded later than the lower structural levels.

Simultaneous exhumation and thrusting within the HHC of Bhutan is depicted schematically in Fig. 7. The arrows above the topography are schematic particle paths for different structural levels within the HHC. The dashed line indicated by the number 1 marks the relative positions of rocks within the HHC at some arbitrary time during thrusting and exhumation. At some point after time 1, the positions of these rocks relative to a fixed Indian shield and Tibet have changed according to the channel flow model discussed in Grujic *et al.* (1996) and are indicated by the number 2. Note that top to the south shearing within the lower and central parts of the HHC is accomplished by adjacent particle paths having different amounts of exhumation over the elapsed time (e.g. the Kakhtang thrust). In addition, top to the north shearing immediately below the STDS leads to normal faulting caused by differential extrusion of material from underneath the ‘Tibetan lid’.

## CONCLUSIONS

Metamorphic reaction textures in the HHC of Bhutan record decompression at high temperatures (c. 600–750 °C) (Fig. 4). The range of temperatures recorded by the decompression reactions and garnet zoning patterns suggest that the HHC experienced decompression while maintaining a laterally heterogeneous, and locally inverted, internal thermal structure. This thermal structure was produced by the thrusting of hot, migmatitic rocks over lower-grade rocks within the HHC (e.g. the Kakhtang thrust, Fig. 1) and by the advection of heat from the intrusion of leucogranite dykes and sills during decompression. The inversion of the metamorphic field gradient near the MCT, however, cannot be used for inferring an inverted

thermal structure at a given instant in time. In-sequence thrusting may result in the propagation of top to the south shearing across the MCTZ and into the footwall of the MCT, thereby passively transporting mineral assemblages formed at earlier times in the structurally higher units. Post-metamorphic transport within the HHC is supported in some areas (e.g. near 93Bp100), where kyanite is deformed and rotated into the top to the south shear foliation (fig. 3b in Swapp & Hollister, 1991).

The range of temperatures maintained within the HHC of Bhutan during decompression appears to contrast with Nepal and parts of India where Hodges *et al.* (1988a) argued that temperatures, based on geothermometry, across large sections of the HHC were nearly uniform. Alternatively, the temperature estimates based on geothermometry may only be reflecting the average blocking temperature for Fe–Mg exchange between garnet and the matrix phases during cooling. This is supported by FeO/(FeO + MgO)-enriched rims present in most of the samples from the Bhutan HHC (Fig. 5). In addition, most garnet from the HHC of Bhutan has complex zoning patterns, variable rim compositions, and in some cases, zoning that is truncated, probably due to garnet resorption during decompression, or fragmentation during deformation. Therefore, most of the rocks in Bhutan are unsuitable for geothermobarometry without careful analysis. This underscores the necessity of determining the spatial composition of rocks using X-ray maps before proceeding with geothermobarometric calculations.

Swapp & Hollister (1991) argued that the migmatites in the upper structural levels of the HHC in Bhutan were tectonically transported (by thrusting) from the deepest parts of the HHC, where temperatures were high enough for melting (due to the breakdown of muscovite and/or biotite under fluid-absent conditions). Rapid decompression of these hot rocks during thrusting and exhumation of the entire HHC probably led to further melting (see Harris & Massey, 1994) and intrusion of leucogranite into the section during top to the south thrusting. All of these processes working in concert: advection of heat due to thrusting and intrusion of leucogranite, rapid decompression at high temperatures and eventually rapid cooling of the HHC, helped cause and preserve the range in temperatures recorded by the metamorphic reaction textures and garnet zoning patterns in the HHC of Bhutan.

Thus, the HHC of Bhutan was extruded and exhumed between the down-going Indian and over-riding Asian plates while being internally deformed by a varying velocity field, rather than being extruded as a rigid block (Fig. 7). The conclusions of Grujic *et al.* (1996), who showed, based on quartz textures, that much of the HHC of Bhutan experienced penetrative top to the south shearing at high temperature, suggested such a model of channel flow between two non-parallel walls.

To conclude, we return to the original compilation of Himalayan geology by Heim & Gansser (1939, p. 225), where, based on field observation and deduction, they made the following statement: 'the crystalline basal part of the Main Central Thrust mass must have been at a depth of 30 km below the surface. There, within (not below) the Sial, at temperatures of 700 °C and more, the injection and migmatization occurred, partly before and partly during the thrusting movement.'

#### ACKNOWLEDGEMENTS

The samples used in this study were collected during the 1993 Swiss–American expedition to Bhutan, which consisted of R. Kündig, D. Grujic, S. Schmid, R. Schmid, T. Pavlis, R. Moseley and L. Hollister. We are grateful to the authorities for permitting us to follow the geology rather than beaten trekkers' paths, and to F. and L. Hoch for their interest in our success. The thorough and constructive reviews from M. Williams and J.-P. Burg are also gratefully acknowledged. The petrology and microprobe work were carried out at Princeton University with the support of NSF grant EAR 9406253 to L.H. C.D. and L.H. are indebted to E. Vicenzi for assistance in obtaining the X-ray images of Fig. 3. The work on leucogranite microstructures was carried out at Basel; C.D. was supported there by Schweizerischer Nationalfonds grants 21–29804.90 and 20–35891.92 to S.S. D.G. acknowledges financial support from the Barth and Karl Kappeler funds from ETH-Zürich.

#### REFERENCES

- Barnicoat, A. C. & Treloar, P. J., 1989. Himalayan metamorphism. *Journal of Metamorphic Geology*, **7**, 3–8.
- Berman, R. G., 1988. Internally consistent thermodynamic data for minerals in the system Na<sub>2</sub>O–K<sub>2</sub>O–CaO–MgO–FeO–Fe<sub>2</sub>O<sub>3</sub>–Al<sub>2</sub>O<sub>3</sub>–SiO<sub>2</sub>–TiO<sub>2</sub>–H<sub>2</sub>O–CO<sub>2</sub>. *Journal of Petrology*, **29**, 445–522.
- Berman, R. G., 1990. Mixing properties of Ca–Mg–Fe–Mn garnets. *American Mineralogist*, **75**, 328–344.
- Berman, R. G., 1991. Thermobarometry using multi-equilibrium calculations: a new technique, with petrological applications. *Canadian Mineralogist*, **29**, 833–855.
- Bouchez, J.-L. & Pêcher, A., 1981. The Himalayan Main Central Thrust pile and its quartz rich tectonites in central Nepal. *Tectonophysics*, **78**, 23–50.
- Bouchez, J.-L., Delas, C., Gleizes, G., Nédélec, A. & Cuney, M., 1992. Submagmatic microfractures in granites. *Geology*, **20**, 35–38.
- Brun, J.-P., Burg, J.-P. & Chen, G. M., 1985. Strain trajectories above the Main Central Thrust (Himalaya) in southern Tibet. *Nature*, **313**, 388–390.
- Brunel, M., 1986. Ductile thrusting in the Himalayas: shear sense criteria and stretching lineations. *Tectonics*, **5**, 247–265.
- Burchfiel, B. C. & Royden, L. H., 1985. North–south extension within the convergent Himalayan region. *Geology*, **13**, 679–682.
- Burchfiel, B. C., Chen, Z., Hodges, K. V., Liu, Y., Royden, L. H., Deng, C. & Xu, J., 1992. The South Tibetan detachment system, Himalayan Orogen: extension contemporaneous with and parallel to shortening in a collisional mountain belt. *Geological Society of America Special Paper*, **269**.

- Burg, J.-P. & Chen, G. M., 1984. Tectonics and structural zonation of southern Tibet, China. *Nature*, **311**, 219–223.
- Burg, J. P., Brunel, M., Gapais, D., Chen, G. M. & Liu, G. H., 1984. Deformation of leucogranites of the crystalline Main Central Sheet in southern Tibet (China). *Journal of Structural Geology*, **6**, 535–542.
- Crawford, M. L., 1974. Calcium zoning in almandine: a model based on plagioclase equilibria. In: *The Feldspars: Proceedings of a NATO Advanced Study Institute*, pp. 629–644. Manchester University Press, Manchester.
- Davidson, C., Rosenberg, C. & Schmid, S. M., 1996. Synmagmatic folding of the base of the Bergell pluton, Central Alps. *Tectonophysics*, **265**, 213–238.
- Deniel, C., Vidal, P., Fernandez, A., Le, F. P. & Peucat, J. J., 1987. Isotopic study of the Manaslu granite (Himalaya, Nepal); inference on the age and source of Himalayan leucogranites. *Contributions to Mineralogy and Petrology*, **96**, 78–92.
- Edwards, M. A., Kidd, W. S. F., Jixiang, L., Yongjun, Y. & Clark, M., 1996. Multi-stage development of the southern Tibet detachment system near Khula Kangri. New data from Gonto La. *Tectonophysics*, **260**, 1–19.
- Ferrara, G., Lombardo, B., Tonarini, S. & Turi, B., 1991. Sr, Nd and O isotopic characterisation of the Gophu La and Gumburanjun leucogranites (High Himalaya). *Schweizerische Mineralogische Petrographische Mitteilungen*, **71**, 35–51.
- Ferry, J. M. & Spear, F. S., 1978. Experimental calibration of the partitioning of Fe and Mg between biotite and garnet. *Contributions to Mineralogy and Petrology*, **66**, 113–117.
- Fitz Gerald, J. D. & Stünitz, H., 1993. Deformation of granitoids at low metamorphic grade. I: Reactions and grain size reduction. *Tectonophysics*, **221**, 269–297.
- Ganguly, J., 1972. Staurolite stability and related parageneses. Theory, experiments, and applications. *Journal of Petrology*, **13**, 335–365.
- Gansser, A., 1964. *The Geology of the Himalayas*. John Wiley & Sons, London.
- Gansser, A., 1983. Geology of the Bhutan Himalaya. *Denkschriften der Schweizerischen Naturforschenden Gesellschaft*, **96**, 1–181.
- Ghent, E. D., 1976. Plagioclase-garnet- $\text{Al}_2\text{SiO}_5$ -quartz: a potential geobarometer-geothermometer. *American Mineralogist*, **61**, 710–714.
- Ghent, E. D. & Stout, M. Z., 1981. Geobarometry and geothermometry of plagioclase-biotite-garnet-muscovite assemblages. *Contributions to Mineralogy and Petrology*, **76**, 92–97.
- Grujic, D., Casey, M., Davidson, C., Hollister, L., Kündig, R., Pavlis, T. & Schmid, S., 1996. Ductile extrusion of the Higher Himalayan Crystalline in Bhutan: Evidence from quartz microstructures. *Tectonophysics*, **260**, 21–43.
- Harris, N., Inger, S. & Massey, J., 1993. The role of fluids in the formation of High Himalayan leucogranites. In: *Himalayan Tectonics* (eds Treloar, P. J. & Searle, M.P.), *Geological Society Special Publication*, **74**, 391–400.
- Harris, N. & Massey, J., 1994. Decompression and anatexis of Himalayan metapelites. *Tectonics*, **13**, 1537–1546.
- Heim, A. & Gansser, A., 1939. Central Himalaya. Geological observations of the Swiss expedn 1936. *Denkschriften der Schweizerischen Naturforschenden Gesellschaft*, **73**, 1–245.
- Hodges, K. V., Hubbard, M. S. & Silverberg, D. S., 1988b. Metamorphic constraints on the thermal evolution of the central Himalayan orogen. *Philosophical Transactions of the Royal Society of London*, **A326**, 257–280.
- Hodges, K. V., Le Fort, P. & Pêcher, A., 1988a. Possible thermal buffering by crustal anatexis in collisional orogens: thermobarometric evidence from the Nepalese Himalaya. *Geology*, **16**, 707–710.
- Hollister, L. S., 1966. Garnet zoning. An interpretation based on the Rayleigh fractionation model. *Science*, **154**, 1647–1650.
- Hubbard, M. S., 1989. Thermobarometric constraints on the thermal history of the Main Central thrust zone and Tibetan Slab, eastern Nepal Himalaya. *Journal of Metamorphic Geology*, **7**, 19–30.
- Jain, A. K. & Manickavasagam, R. M., 1993. Inverted metamorphism in the intracontinental ductile shear zone during Himalayan collision tectonics. *Geology*, **21**, 407–410.
- Jamieson, R. A., Beaumont, C., Hamilton, J. & Fullsack, P., 1996. Tectonic assembly of inverted metamorphic sequences. *Geology*, **24**, 839–842.
- Jaupart, C. & Provost, A., 1985. Heat focusing, granite genesis, and inverted metamorphic gradients in continental collision zones. *Earth and Planetary Science Letters*, **73**, 385–397.
- John, B. E. & Blundy, J. D., 1993. Emplacement-related deformation of granitoid magmas, southern Adamello Massif, Italy. *Geological Society of America Bulletin*, **105**, 1517–1541.
- Kretz, R., 1983. Symbols for rock-forming minerals. *American Mineralogist*, **68**, 277–279.
- Lang, H. M. & Rice, J. M., 1985. Regression modelling of metamorphic reactions in metapelites, Snow Peak, northern Idaho. *Journal of Petrology*, **26**, 857–887.
- Le Fort, P., 1975. Himalaya: the collided range. Present knowledge of the continental arc. *American Journal of Science*, **275 A**, 1–44.
- Le Fort, P., Cuney, M., Deniel, C., France-Lanord, C., Sheppard, S. M. F., Upreti, B. N. & Vidal, P., 1987. Crustal generation of the Himalayan leucogranites. *Tectonophysics*, **134**, 39–57.
- Loomis, T. P., 1978. Multicomponent diffusion in garnet: II. Comparison of models with natural data. *American Journal of Science*, **278**, 1119–1137.
- Maluski, H., Matte, P., Brunel, M. & Xiao, X., 1988. Argon 39 – argon 40 dating of metamorphic and plutonic events in the North and High Himalaya belts (southern Tibet, China). *Tectonics*, **7**, 299–326.
- McMullin, D. W., Berman, R. G. & Greenwood, H. J., 1991. Calibration of SGAM thermobarometer for pelitic rocks using data from phase equilibrium experiments and natural assemblages. *Canadian Mineralogist*, **29**, 889–908.
- Mohan, A., Windley, B. F. & Searle, M. P., 1989. Geothermobarometry and development of inverted metamorphism in the Darjeeling-Sikkim region of the eastern Himalaya. *Journal of Metamorphic Geology*, **7**, 95–110.
- Pêcher, A., 1989. The metamorphism in the central Himalaya. *Journal of Metamorphic Geology*, **7**, 31–41.
- Pigay, L. C., 1976. Metamorphism of the Settler Schist, southwest of Yale, British Columbia. *Canadian Journal of Earth Sciences*, **13**, 405–421.
- Reddy, S. A., Searle, M. P. & Massey, J. A., 1993. Structural evolution of the High Himalayan gneiss sequence, Langtang Valley, Nepal. In: *Himalayan Tectonics* (eds Treloar, P. J. & Searle, M.P.), *Geological Society Special Publication*, **74**, 375–389.
- Scaillet, B., Pichavant, M. & Holtz, F., 1995. Experimental constraints on the petrogenesis of the High Himalayan leucogranites. *10th Himalaya Karakoram Tibet Workshop, Monte Verita, Ascona, Ticino, Switzerland, 4–8 April, 1995, Abstract Volume: Zürich, Switzerland. Mitteilungen aus dem Geologischen Institut der Eidgenössischen Technischen Hochschule und der Universität Zürich*, **298**, 124–127.
- Searle, M. P., Cooper, D. J. W. & Rex, A. J., 1988. Collision tectonics of the Ladakh-Zaskar Himalaya. *Philosophical Transactions of the Royal Society of London*, **A326**, 117–150.
- Searle, M. P. & Rex, A. J., 1989. Thermal model for the Zaskar Himalaya. *Journal of Metamorphic Geology*, **7**, 127–134.
- Searle, M. P., Waters, D. J., Rex, D. C. & Wilson, R. N., 1992. Pressure, temperature and time constraints on Himalayan metamorphism from eastern Kashmir and western Zaskar. *Journal of the Geological Society of London*, **149**, 753–773.
- Spear, F. S., 1991. On the interpretation of peak metamorphic temperatures in light of garnet diffusion during cooling. *Journal of Metamorphic Geology*, **9**, 379–388.
- Swapp, S. M. & Hollister, L. S., 1991. Inverted metamorphism within the Tibetan slab of Bhutan: evidence for a tectonically transported heat-source. *Canadian Mineralogist*, **29**, 1019–1041.

- Tracy, R. J., 1982. Compositional zoning and inclusions in metamorphic minerals. In: *Characterization of Metamorphism through Mineral Equilibria* (ed. Ferry, J.M.), *Mineralogical Society of America, Reviews in Mineralogy*, **10**, 355–397.
- Tracy, R. J., Robinson, P. & Thompson, A. B., 1976. Garnet composition and zoning in the determination of temperature and pressure of metamorphism, central Massachusetts. *American Mineralogist*, **61**, 762–775.
- Treloar, P. J. & Searle, M. P., 1993. *Himalayan Tectonics*. Geological Society Special Publication 74, Oxford.
- Windley, B. F., 1983. Metamorphism and tectonics of the Himalaya. *Journal of the Geological Society of London*, **140**, 849–865.
- Woodsworth, G. J., 1977. Homogenization of zoned garnets from pelitic schists. *Canadian Mineralogist*, **15**, 230–242.
- Yardley, B. W. D., 1977. An empirical study of diffusion in garnet. *American Mineralogist*, **62**, 793–800.

*Received 23 May 1996; revision accepted 30 January 1997.*